NASA Technical Memorandum 84499

METHODOLOGY FOR DETERMINING ELEVON DEFLECTIONS TO TRIM AND MANEUVER THE DAST VEHICLE WITH NEGATIVE STATIC MARGIN

BOYD PERRY III

MAY 1982

National Aeronautics and Space Administration

Langley Research Center
Hampton, Virginia 23665

CONTENTS

INTRODUCTION

The NASA Drones for Aerodynamic and Structural Testing (DAST) program uses a remotely-piloted Firebee II drone vehicle to flight test aeroelastic research wings (ARW). The second such wing, ARW-2, will have an active control system which will perform multiple active control functions simultaneously. One of these functions is relaxed static stability (RSS). The RSS concept eliminates the requirement for inherent airplane stability (ref. 1) (inherent stability being described in terms of the static margin, the normalized distance--relative to the mean aerodynamic chord (m.a.c.)--between the vehicle center of gravity and neutral point). The "relaxed" inherent stability is augmented by the active control system. At its inherently-most-unstable flight condition, the ARW-2 configuration will have a static margin on the order of -10 percent of the m.a.c.

In preparation for selecting future research wings in the DAST program, the question of the maximum allowable negative static margin is being considered. Can the Firebee II drone vehicle, with its standard elevons, but fitted with a new research wing and a new active control system, be trimmed and maneuvered with a static margin of -15 percent? This question can only be answered with certainty if detailed information about the new wing and new active control system is known. At this time, this information is not known.

Acknowledging that there is insufficient information to answer the static-margin question for a new wing and active control system, the purpose of this paper is to present both the methodology that will be required to answer the question when the information is known and the application of this methodology to a research wing. Because of the extensive amount of data available for the ARW-2 configuration and because the ARW-2 wing is representative of a class of wings envisioned for future flight tests in the DAST program (supercritical airfoil, low sweep, high aspect ratio), the ARW-2 configuration will be used to assess the methodology.

SYMBOLS

The results presented herein are referred to the stability-axis system. All dimensional values are given in SI Units; however, calculations were made in U.S. Customary Units.

b	wing span, m
C_L	lift coefficient, $\frac{\text{Lift}}{qS}$
C_ℓ	rolling-moment coefficient, $\frac{\text{Rolling moment}}{qSb}$, positive right wing down
C_m	pitching-moment coefficient, $\frac{\text{Pitching moment}}{qS\bar{c}}$, positive nose up
$C_{m_{o_i}}$	zero-lift pitching moment for elevon deflection "i"
$C_{m_{o_o}}$	zero-lift pitching moment for zero elevon deflection
C_n	yawing-moment coefficient, $\frac{\text{Yawing moment}}{qSb}$, positive nose right
C_y	side-force coefficient, $\frac{\text{Side force}}{qS}$, positive right
C_z	vertical-force coefficient, $\frac{\text{Vertical force}}{qS}$, positive down
$\bar{c}$	wing mean aerodynamic chord, m
$F_A(s)$	actuator transfer function
$F_c(s)$	column transfer function
$F_i(s)$	feedback transfer function; $i = 1, 2, \ldots, n$
g	acceleration due to gravity, m/sec^2
$g_{ij}(s)$	coefficient polynomials; $i = 1, 2$; $j = 1, 2$. See eq. (13).
h	airplane center of gravity position expressed as a fraction of $\bar{c}$
h_n	airplane neutral point position expressed as a fraction of $\bar{c}$
I_{xx}	vehicle roll moment of inertia, $kg\text{-}m^2$
I_{xz}	vehicle roll-yaw product of inertia, $kg\text{-}m^2$
I_{yy}	vehicle pitch moment of inertia, $kg\text{-}m^2$
I_{zz}	vehicle yaw moment of inertia, $kg\text{-}m^2$

i_A nondimensional I_{xx}, $\frac{I_{xx}}{\rho S(b/2)^3}$

i_B nondimensional I_{yy}, $\frac{I_{yy}}{\rho S(\bar{c}/2)^3}$

i_C nondimensional I_{zz}, $\frac{I_{zz}}{\rho S(b/2)^3}$

i_E nondimensional I_{xz}, $\frac{I_{xz}}{\rho S(b/2)^3}$

K_c, K_α, K_q feedback gains for simplified RSS. See fig. 5.

K_1, K_2 feedback gains for lateral-directional AFCS. See fig. 7.

m airplane mass, kg

n acceleration factor, g units

p roll rate, positive right wing down

q pitch rate, positive nose up

$\bar{q}$ dynamic pressure, $\frac{1}{2}\rho V^2$

r yaw rate, positive nose right

r_i response quantity; i = 1, 2, ..., n. See sketch on page 12.

S wing area, m^2

s Laplace variable

t time, seconds

t^* longitudinal characteristic time, $\frac{\bar{c}/2}{V}$

t^* lateral-directional characteristic time, $\frac{b/2}{V}$

V airplane true airspeed, m/sec

α airplane total angle of attack

α_{0_i} zero-lift angle of attack for elevon deflection "i"

α_{o_o} zero-lift angle of attack for zero elevon deflection

β sideslip angle, positive nose left

δ collective elevon deflection angle, positive trailing edge down

δ_d differential elevon deflection angle, $1/2(\delta_R-\delta_L)$, positive to produce a roll right wing up

δ_n collective elevon deflection for n-g pull-up

δ_r rudder deflection angle, positive trailing edge left

δ_L deflection angle of left elevon, positive trailing-edge down. See eq. (14).

δ_R deflection angle of right elevon, positive trailing-edge down. See eq. (14).

δ_{trim} collective elevon deflection angle to achieve trimmed 1g straight-and-level flight

δ_{column} deflection of control column, positive for pull up

δ_{wheel} deflection of control wheel, positive for roll right wing up

$\Delta\delta$ incremental collective elevon deflection for (n-1)g pull up

Δ appearing before another quantity, indicates a perturbation of that quantity

ζ damping ratio

μ longitudinal mass ratio, $\frac{m}{\rho S(\bar{c}/2)}$

μ lateral-directional mass ratio, $\frac{m}{\rho S(b/2)}$

ρ air density, kg/m^3

ϕ roll angle, positive right wing down

ψ yaw angle, positive nose right

ω_d dumped natural frequency, rad/sec

$$C_{m_\alpha} = \frac{\partial C_m}{\partial \alpha} \qquad C_{z_\alpha} = \frac{\partial C_z}{\partial \alpha} \qquad C_{L_\alpha} = \frac{\partial C_L}{\partial \alpha}$$

$$C_{m_{\dot{\alpha}}} = \frac{\partial C_m}{\partial (\frac{\dot{\alpha}\bar{c}}{2V})} \qquad C_{z_{\dot{\alpha}}} = \frac{\partial C_z}{\partial (\frac{\dot{\alpha}\bar{c}}{2V})}$$

$$C_{m_q} = \frac{\partial C_m}{\partial \left(\frac{qc}{2V}\right)} \qquad C_{z_q} = \frac{\partial C_z}{\partial \left(\frac{qc}{2V}\right)} \qquad C_{L_q} = \frac{\partial C_L}{\partial \left(\frac{qc}{2V}\right)}$$

$$C_{m_\delta} = \frac{\partial C_m}{\partial \delta} \qquad C_{z_\delta} = \frac{\partial C_z}{\partial \delta}$$

$$C_{y_\beta} = \frac{\partial C_y}{\partial \beta} \qquad C_{\ell_\beta} = \frac{\partial C_\ell}{\partial \beta} \qquad C_{n_\beta} = \frac{\partial C_n}{\partial \beta}$$

$$C_{y_p} = \frac{\partial C_y}{\partial \left(\frac{pb}{2V}\right)} \qquad C_{\ell_p} = \frac{\partial C_\ell}{\partial \left(\frac{pb}{2V}\right)} \qquad C_{n_p} = \frac{\partial C_n}{\partial \left(\frac{pb}{2V}\right)}$$

$$C_{y_r} = \frac{\partial C_y}{\partial \left(\frac{rb}{2V}\right)} \qquad C_{\ell_r} = \frac{\partial C_\ell}{\partial \left(\frac{rb}{2V}\right)} \qquad C_{n_r} = \frac{\partial C_n}{\partial \left(\frac{rb}{2V}\right)}$$

$$C_{y_{\delta_d}} = \frac{\partial C_y}{\partial \delta_d} \qquad C_{\ell_{\delta_d}} = \frac{\partial C_\ell}{\partial \delta_d} \qquad C_{n_{\delta_d}} = \frac{\partial C_n}{\partial \delta_d}$$

$$C_{y_{\delta_r}} = \frac{\partial C_y}{\partial \delta_r} \qquad C_{\ell_{\delta_r}} = \frac{\partial C_\ell}{\partial \delta_r} \qquad C_{n_{\delta_r}} = \frac{\partial C_\ell}{\partial \delta_r}$$

Subscripts and abbreviations

trim	1g straight-and-level flight
AFCS	automatic flight control system
ARW-2	aeroelastic research wing number 2
DAST	drones for aerodynamic and structural testing
peak	maximum or minimum value
RSS	relaxed static stability

DESCRIPTION OF DAST VEHICLE AND ELEVON

A drawing of the DAST vehicle (fitted with the ARW-2 wing) is shown at the top of figure 1. On this vehicle, pitch and roll control are accomplished using the all-moving horizontal tail (elevon). A detail drawing of the elevon and a table of pertinent geometric characteristics are presented in the bottom portion of the figure. The elevon is configured to deflect collectively for pitch control and differentially for roll control according to the envelope of maximum limits shown in figure 2. From figure 2, the current maximum available limits for elevon deflection are 7 degrees trailing-edge down and 12 degrees trailing-edge up.

APPROACH

The methodology described in this paper is developed to answer the question: At -15% static margin, are the current limits on elevon deflection adequate to: (1) trim the vehicle in 1g straight-and-level flight, (2) perform required longitudinal maneuvers, and (3) perform required lateral maneuvers? Possible sources of elevon deflections are commands by the active control system and the pilot. For the purpose of this paper it is assumed that relaxed static stability is the only active control function provided by the active control system. Functions such as gust and maneuver load alleviation (which, in addition to RSS, could also send commands to the elevon) are not considered.

Therefore, to determine if the current limits (positive and negative) on elevon deflection are adequate, the following approach is taken:

Step 1: Determine the elevon deflection required to trim the vehicle in 1g straight-and-level flight.

Step 2: Determine the incremental elevon deflection required to perform an incremental 1.5g pull-up maneuver. Add this incremental deflection to the trim deflection determined in Step 1.

Step 3: Determine the incremental elevon deflection required to meet the MIL SPEC (ref. 2) for roll performance. Add this incremental deflection to the trim deflection determined in Step 1.

The results of Steps 1, 2 and 3 are compared with the current deflection limits at several representative flight conditions.

METHODOLOGY

This section of the paper presents the equations necessary to compute the various types of elevon deflection specified in the Approach section. The methodology presented in this section of the paper is composed of several

parts, or components, all of which are well understood and discussed in numerous textbooks: static stability and control, dynamic stability and control, and elements of classical control theory. Even though these various components are not new, in this paper they are linked together in a manner that emphasizes the relationships between elevon deflection and the static margin of the vehicle. This linking together and emphasis are what is referred to in this paper as "methodology."

Assumptions

The methodology presented in this paper is, by choice, based on certain assumptions which simplify the analyses considerably but which, at the same time, retain the essential features of the problem. The following is a list and brief discussion of these simplifying assumptions.

1. Flexible degrees of freedom are not considered in the analysis. However, the effects of such flexibility are incorporated through "elastic corrections" to the rigid-body stability derivatives.

2. The airplane equations of motion are linearized with respect to a reference condition of steady flight. This linearization is the result of the assumption that airplane motions consist of "small" deviations from the reference flight condition. As a consequence of the linearization, the longitudinal and lateral-directional degrees of freedom are decoupled.

3. It is further assumed that the longitudinal motions of the airplane are adequately described by the short-period approximation to the longitudinal equations. Implicit in this assumption is that the phugoid mode is stable.

4. It is assumed that steady-state elevon angles required to achieve 1g trim and to perform steady pull-up maneuvers can be calculated adequately by examining vehicle equilibrium only, and not vehicle motion. This is referred to as static stability and control in reference 3.

Elevon Deflection for Trim

The following is a derivation of the elevon deflection required to trim the vehicle in 1g straight-and-level flight. It is based on the information presented in Chapter 2 of reference 3 and the following sketch:

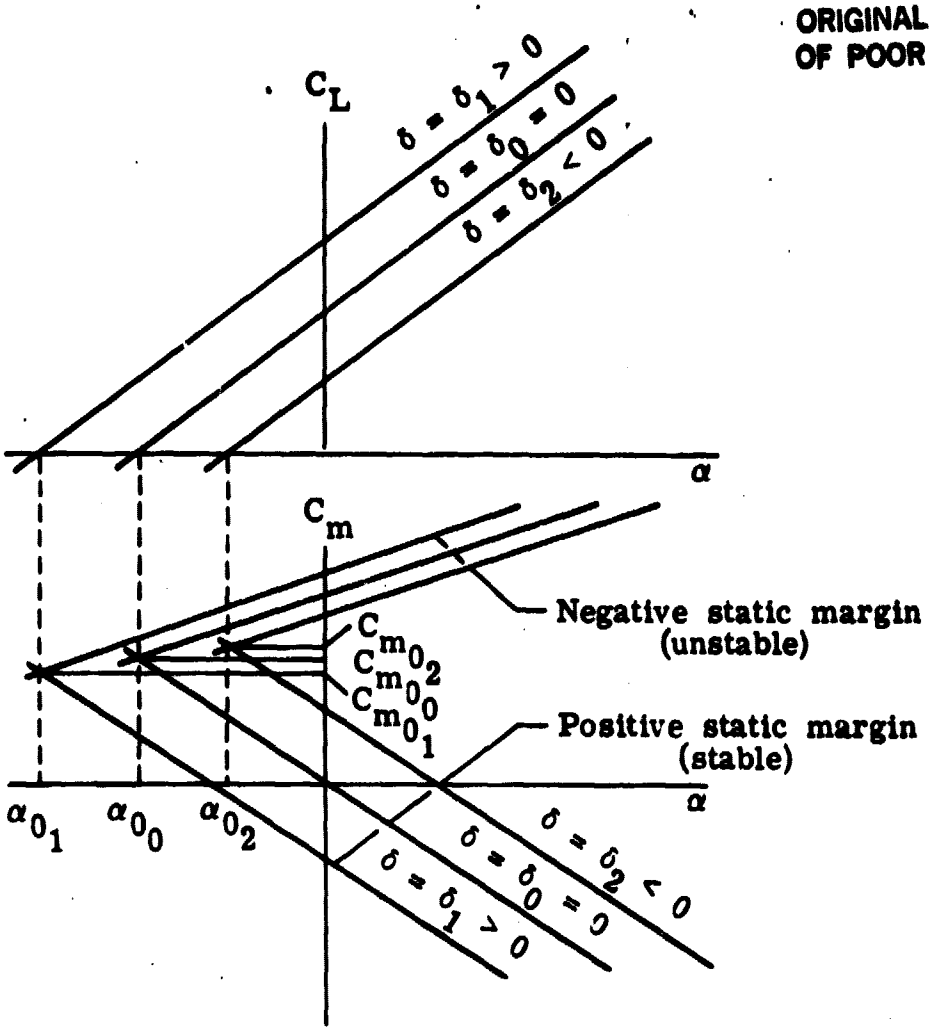

The sketch illustrates the effects of varying elevon deflection and static margin on the lift coefficient and pitching-moment coefficient curves. Assumptions implicit in the sketch are that:

1. The C_L vs. α and C_m vs. α curves are described by straight lines.

2. Changes in elevon deflection, δ, translate the C_L vs. α and C_m vs. α curves parallel to their zero-deflection curves, resulting in new zero-lift angles of attack, α_{0_1}, and new zero-lift pitching moments, $C_{m_{0_1}}$.

3. Changes in static margin, (h_n-h), rotate the C_m vs. α curves about their zero-lift pitching moment, but have no effect on the C_L vs. α curves.

4. The variations of α_o and C_{m_o} with δ are constant, that is

$$\frac{\partial \alpha_o}{\partial \delta} \text{ and } \frac{\partial C_{m_o}}{\partial \delta}$$

are constants.

5. The variation of the slope of the C_m vs. α curve with static margin is constant and expressed by

$$C_{m_\alpha} = -C_{L_\alpha}(h_n - h)$$

Referring to the sketch, equations for lift coefficient and pitching-moment coefficient can be written for any α, δ, and (h_n-h). Lift coefficient is a function of angle of attack, α, elevon deflection angle, δ, and the zero-lift zero-elevon-deflection angle of attack, α_{o_o}:

$$C_L = C_{L_\alpha}(\alpha - \alpha_{o_o}) + C_{L_\delta}\delta \tag{1}$$

Pitching moment coefficient is a function of α, δ, α_{o_o}, static margin, (h_n-h), and zero-lift zero-elevon-deflection moment coefficient, $C_{m_{o_o}}$:

$$C_m = C_{m_{o_o}} + C_{m_\alpha}(\alpha - \alpha_{o_o}) + C_{m_\delta}\delta \tag{2}$$

$$\text{where } C_{m_\delta} = \frac{\partial C_{m_o}}{\partial \delta} + C_{m_\alpha}\frac{C_{L_\delta}}{C_{L_\alpha}}$$

At trim, $C_m=0$ and lift coefficient, angle of attack, and elevon deflection angle attain their "trim values" $C_{L_{trim}}$, α_{trim}, δ_{trim}. Therefore, at trim equations (1) and (2) can be re-written as

$$C_{L_{trim}} = C_{L_\alpha}(\alpha_{trim} - \alpha_{o_o}) + C_{L_\delta}\delta_{trim} \tag{3}$$

$$0 = C_{m_{o_o}} + C_{m_\alpha}(\alpha_{trim} - \alpha_{o_o}) + \left(\frac{\partial C_{m_o}}{\partial \delta} + C_{m_\alpha}\frac{C_{L_\delta}}{C_{L_\alpha}}\right)\delta_{trim} \tag{4}$$

Making use of the substitution $C_{m_\alpha} = C_{L_\alpha}(h-h_n)$, the expression for δ_{trim} is obtained by solving equations (3) and (4) simultaneously,

$$\delta_{trim} = \frac{(h_n-h)C_{L_{trim}} - C_{m_o}}{\frac{\partial C_{m_o}}{\partial \delta}} \tag{5}$$

To determine if the trim deflection is within available limits, the value of δ_{trim} obtained from equation (5) is compared with those limits.

Elevon Deflection for Pull-up Maneuver

This section presents equations for the incremental elevon deflection, $\Delta\delta$, necessary to trim the vehicle in a steady pull-up maneuver of incremental load factor n-1. The total elevon deflection necessary for a pull up of load factor is n is found by taking the sum

$$\delta_n = \delta_{trim} + \Delta\delta \tag{6}$$

Steady-state elevon deflection.- The following derivation is based on the information presented in Chapter 3 of reference 3. It is assumed that the airplane is trimmed in a steady (unaccelerating) pull up of incremental load factor n-1. With respect to 1g straight-and-level flight, the incremental lift (ΔC_L) and pitching moment (ΔC_m) for this maneuver may be written as

$$\Delta C_L = \frac{\partial C_L}{\partial \alpha}\Delta\alpha + \frac{\partial C_L}{\partial \delta}\Delta\delta + \frac{\partial C_L}{\partial q}\Delta q \tag{7}$$

$$\Delta C_m = \frac{\partial C_m}{\partial \alpha}\Delta\alpha + \frac{\partial C_m}{\partial \delta}\Delta\delta + \frac{\partial C_m}{\partial q}\Delta q \tag{8}$$

where $\Delta\alpha$, $\Delta\delta$, and Δq are the incremental values from α_{trim}, δ_{trim}, and q_{trim} ($q_{trim}=0$). Because the maneuver is unaccelerating in pitch, the incremental pitching moment is zero. Equations (7) and (8) are solved simultaneously for $\Delta\delta$ after the following substitutions are made:

$$\Delta C_L = (n-1)C_{L_{trim}}$$

$$\frac{\partial C_L}{\partial \alpha} = C_{L_\alpha}, \quad \frac{\partial C_L}{\partial \delta} = C_{L_\delta}, \quad \frac{\partial C_L}{\partial q} = \frac{\bar{c}}{2V} C_{L_q}$$

$$\frac{\partial C_m}{\partial \alpha} = C_{m_\alpha}, \quad \frac{\partial C_m}{\partial \delta} = C_{m_\delta}, \quad \frac{\partial C_m}{\partial q} = \frac{\bar{c}}{2V} C_{m_q}$$

$$\Delta q = \frac{(n-1)g}{V}$$

resulting in:

$$\Delta\delta = (n-1)\frac{(h_n-h)\left(C_{L_{trim}} - C_{L_q}\frac{\bar{c}q}{2V^2}\right) - C_{m_q}\frac{\bar{c}q}{2V^2}}{\frac{\partial C_{m_0}}{\partial \delta}} \qquad (9)$$

The total steady-state value of elevon deflection for a 2.5g pull-up maneuver is obtained by substituting equations (5) and (9) (with $n = 2.5$) into equation (6). To determine if this value is within available limits, it is compared with those limits.

Time-varying elevon deflection.- Equation (5) is the value of elevon deflection necessary to trim the airplane in 1g straight-and-level flight. Equation (9) is the value necessary to trim the vehicle in a steady pull up. Both describe steady-state conditions. To proceed from the condition of 1g steady-state flight (with $\delta = \delta_{trim}$) to the condition of n-g's steady-state flight (with $\delta = \delta_{trim} + \Delta\delta$) requires that $\Delta\delta$ (and therefore δ) vary in some manner with time. This time-varying behavior of $\Delta\delta$ may be computed by solving the airplane longitudinal dynamic equations of motion. These dynamic equations of motion are functions of the airplane aerodynamic and inertia characteristics and the characteristics of the active control system for RSS. This section describes how the time-varying behavior in $\Delta\delta$ is obtained.

Because the characteristics of the active control system for RSS are not known, the dynamic equations of motion can only be given in general form. The block diagram in the following sketch represents a "general" RSS active control system.

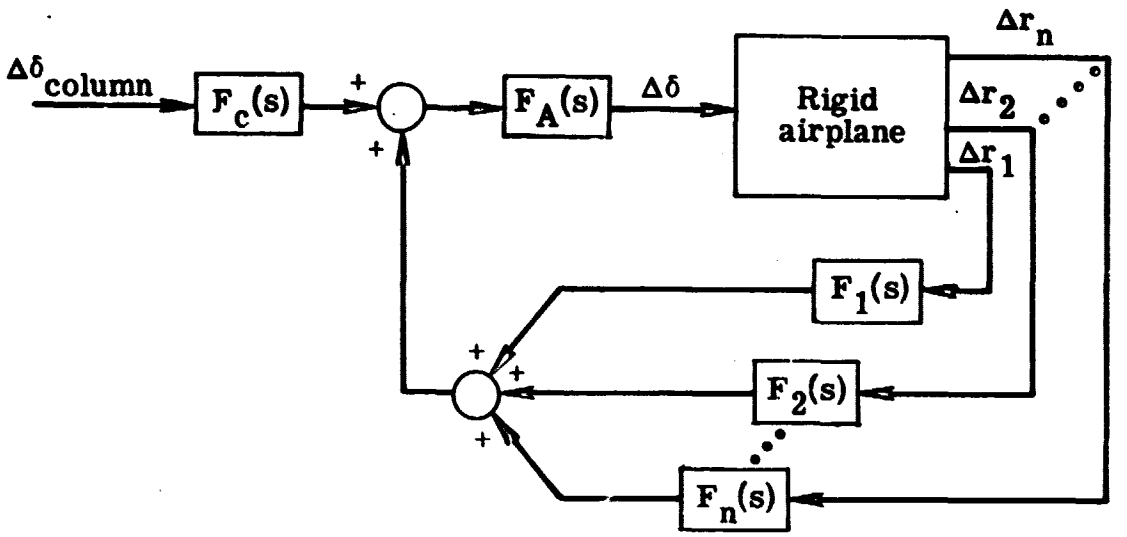

It features incremental column input through transfer function $F_c(s)$ and "n" feedback loops (involving incremental response quantities Δr_1, Δr_2, ..., Δr_n through transfer functions $F_1(s)$, $F_2(s)$, ..., $F_n(s)$, respectively). The input and feedback signals are summed at the top summing junction. The resultant signal passes through an actuator transfer function $F_A(s)$, resulting in the incremental elevon deflection $\Delta\delta$. The box labelled "rigid airplane" contains the short-period approximation to the longitudinal equations of motion. These equations (from Chapter 4 of ref. 3) are written below with elevon deflection on the right-hand side

$$\left.\begin{aligned} (2\mu t^* - C_{Z_{\dot\alpha}} t^*)\Delta\dot\alpha - C_{Z_\alpha}\Delta\alpha - (2\mu t^* - C_{Z_q} t^*)\Delta q &= C_{Z_\delta}\Delta\delta \\ -C_{m_{\dot\alpha}} t^*\Delta\dot\alpha - C_{m_\alpha}\Delta\alpha + i_B t^{*2}\Delta\dot q - C_{m_q} t^*\Delta q &= C_{m_\delta}\Delta\delta \end{aligned}\right\} \qquad (10)$$

Equations (10) are linear ordinary simultaneous differential equations in the time domain, where the quantities $\Delta\alpha$, $\Delta\dot\alpha$, Δq, $\Delta\dot q$, and $\Delta\delta$ are perturbations away from the condition of 1g trimmed flight. Referring again to the block diagram, one of the incremental response quantities, Δr_i, may be the incremental load factor, Δn, whose equation is given by

$$\Delta n = \frac{V}{g}(\Delta q - \Delta \dot{\alpha}) \tag{11}$$

The following equation is written in the Laplace domain and represents the condition at the top summing junction in the block diagram

$$\Delta\delta = F_A(s)[F_c(s)\Delta\delta_{column} + F_1(s)\Delta r_1 + F_2(s)\Delta r_2 + \cdots + F_n(s)\Delta r_n] \tag{12}$$

where the responses, Δr_i, are combinations of $\Delta\alpha$, Δq and their time derivatives. Equations for the entire block diagram are obtained by substituting equation (12) into the Laplace transform of equation (10). After substitution, the resulting equations are manipulated algebraically, leaving only terms containing $\Delta\delta_{column}$ on the right-hand side. Equation (13) shows the form of the resulting equations

$$\left.\begin{aligned} g_{11}(s)\Delta\alpha + g_{12}(s)\Delta q &= C_{z_\delta} F_c(s) F_A(s)\Delta\delta_{column} \\ g_{21}(s)\Delta\alpha + g_{22}(s)\Delta q &= C_{m_\delta} F_c(s) F_A(s)\Delta\delta_{column} \end{aligned}\right\} \tag{13}$$

After solution of equation (13) there must be appropriate transformation back into the time domain.

The time-varying behavior of δ is found by performing the following steps:

Step 1: Select an appropriate function for $\Delta\delta_{column}$ such that, after solution of equation (13), the desired steady-state value of incremental load factor is obtained from equation (11).

Step 2: Solve for $\Delta\delta$ by substituting $\Delta\delta_{column}$ (from Step 1) and the appropriate responses (from solution of eq. (13)) into equation (12).

Step 3: According to equation (6), add the value of δ_{trim} to each value of $\Delta\delta$ in the time history.

The time history of elevon deflection, which results from Step 3, is then compared to the available limits. This comparison will indicate if the transient elevon deflections exceed the available limits.

Two items of interest should be noted here. The first is that, for a pull-up maneuver of steady-state, incremental load factor n-1, the steady-state value of $\Delta\delta$ from the solution of equations (12) and (13) is the same as that predicted by equation (9). The second is that, at certain flight conditions

and for particular transfer functions $F_C(s)$, $F_A(s)$, $F_1(s)$, ..., $F_n(s)$ in the block diagram, the predicted steady-state value of δ (eq. (6)) for a pull up may be within available limits while the predicted transient values of δ may exceed available limits. This situation emphasizes the need to examine time responses of δ (and not rely solely on the steady-state values) to determine if the available limits are adequate.

Elevon Deflection for Roll Maneuver

This section presents the equations for the incremental differential elevon deflection, $\Delta\delta_d$, necessary to perform required roll maneuvers. Such roll maneuvers are specified in the MIL SPEC on flying qualities (ref. 2). For the DAST vehicle with a research wing being flown as a transport, the specification is that the vehicle be able to roll 30° in 3 seconds (implying that a time-varying analysis is required). That is, there must be sufficient differential elevon deflection available to perform this maneuver. Before the maneuver, the right and left elevons are assumed to be deflected at their trim values for 1g straight-and-level flight. For each elevon, the total elevon deflection is the sum of the trim deflection and the differential deflection required by the maneuver, as indicated in the following equation.

$$\left.\begin{aligned} \delta_R &= \delta_{trim} + \Delta\delta_d \\ \delta_L &= \delta_{trim} - \Delta\delta_d \end{aligned}\right\} \tag{14}$$

In equation (14), δ_{trim} is obtained from equation (5), and $\Delta\delta_d$ comes from the airplane lateral-directional dynamic equations of motion. These equations (from Chapter 4 to ref. 3) are written below retaining, for generality, rudder deflection on the right hand side.

$$\left.\begin{aligned} 2\mu t^*\Delta\dot{\beta} - C_{y_\beta}\Delta\beta - C_{y_p}t^*\Delta p + (2\mu - C_{y_r})t^*\Delta r - C_{L_{trim}}\Delta\dot{\phi} &= C_{y_{\delta_d}}\Delta\delta_d + C_{y_{\delta_r}}\Delta\delta_r \\ -C_{\ell_\beta}\Delta\beta + i_A t^{*2}\Delta\dot{p} - C_{\ell_p}t^*\Delta p - i_E t^{*2}\Delta\dot{r} - C_{\ell_r}t^*\Delta r &= C_{\ell_{\delta_d}}\Delta\delta_d + C_{\ell_{\delta_r}}\Delta\delta_r \\ -C_{n_\beta}\Delta\beta - i_E t^{*2}\Delta\dot{p} - C_{n_p}t^*\Delta p + i_C t^{*2}\Delta\dot{r} - C_{n_r}t^*\Delta r &= C_{n_{\delta_d}}\Delta\delta_d + C_{n_{\delta_r}}\Delta\delta_r \\ \Delta p - \Delta\dot{\phi} &= 0 \\ \Delta r - \Delta\dot{\psi} &= 0 \end{aligned}\right\} \tag{15}$$

These equations are simultaneous linear differential equations in variables $\Delta\beta$, Δp, Δr, $\Delta\phi$, and $\Delta\psi$ with $\Delta\delta_d$ and $\Delta\delta_r$ as forcing functions. The variables and their time derivatives and the forcing functions in equation (15) are all perturbations of these quantities away from their respective trim values.

The time-varying behavior of roll angle ($\Delta\phi$) and differential elevon deflection ($\Delta\delta_d$) are found by:

Step 1: Given the value of trim elevon deflection, determining (by use of fig. 2) the amount of differential deflection remaining for full available differential deflection of the elevon.

Step 2: Inputting the appropriate (time-varying) function (from ref. 2) and magnitude (from Step 1) of $\Delta\delta_d$ into the right-hand side of equation (15).

Step 3: Solving equation (14) for $\Delta\phi$.

The time history of $\Delta\phi$ resulting from Step 3 is then examined to see if the MIL SPEC is satisfied (30° of roll in 3 seconds).

It has been assumed in these analyses that the longitudinal and lateral-directional "sets" of equations are completely decoupled. That is, disturbances in the degrees of freedom of one set create neither aerodynamic nor inertia forces and moments in the other set. As a consequence of this assumption, the active control system for RSS does not need to be considered or included in the solution of the lateral-directional equations. In addition, for the longitudinal equations, differential deflections of the elevon have no effect on the longitudinal trim of the vehicle.

NUMERICAL EXAMPLES

This section of the paper applies the methodology presented in the previous section to the ARW-2 configuration. Elevon deflections are computed (according to eqs. (5), (9), (12), and (14)) and then compared to the available deflection limits at five flight conditions. These conditions are typical of those at which flight tests of ARW-2 will be conducted, and, consequently, the computed elevon deflections will be representative of those expected in flight.

Flight Conditions and Numerical Data

The five flight conditions are depicted by points 1 through 5 in the altitude vs. Mach number plot in figure 3. Starting at the point labelled "cruise condition" and moving vertically down, each successive point doubles dynamic pressure at constant Mach number. Moving diagonally upward from point 4, each

successive point increases Mach number by 0.1 at constant dynamic pressure. The information in Table I defines each point in figure 3 in terms of Mach number, dynamic pressure and altitude. Point 6 in figure 3 and Table I represents the flight condition at which an additional analysis is performed; this analysis is discussed in the appendix.

To perform the numerical examples, stability derivatives and other aerodynamic coefficients, geometric data, and mass and inertia information are required at each of the flight conditions listed in Table I. The aerodynamic data was obtained by interpolating and cross plotting the data presented in two unpublished studies of the ARW-2 configuration. Tables II, III, and IV present this numerical data. Table II contains the data necessary to compute the steady-state values of elevon deflection for 1g straight-and-level flight and for a 2.5g pull-up maneuver. Table III contains the data necessary to compute the time history of elevon deflection as the vehicle changes from the condition of 1g steady-state flight to the condition of a 2.5g steady-state pull up. Table IV contains the data necessary to compute the time history of elevon deflection during the MIL-SPEC roll maneuver.

Nonlinear Pitching Moment Characteristics

At many flight conditions, the ARW-2 pitching moment exhibits a very nonlinear behavior as a function of angle of attack. At low values of angle of attack (values which would be attained in performing only moderate longitudinal maneuvers) the slope of the C_m vs. α curve becomes positive. Then, depending on the flight condition, this slope may become negative again at higher angles of attack. The following sketch of pitching moment as a function of angle of attack illustrates this nonlinear behavior

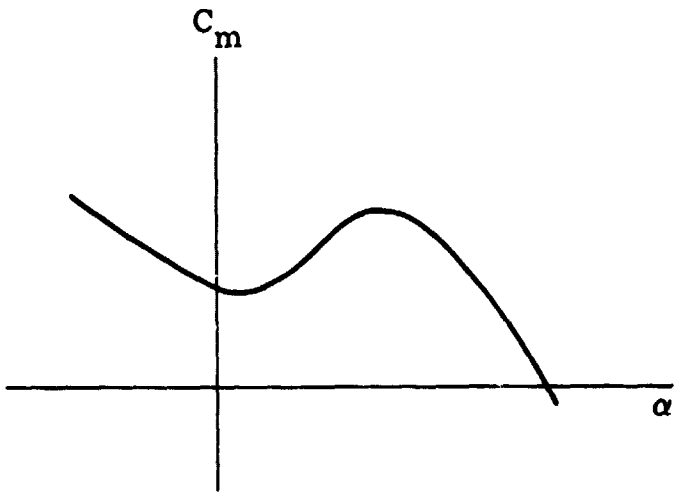

As stated in the assumptions section of this paper, it has been assumed that the airplane forces and moments are linear with respect to deviations in the motion variables (angle of attack being one) from their values at the

reference flight condition. Because pitching moment is not linear with respect to angle of attack for the ARW-2 configuration, this assumption introduces some error into the numerical results presented in the examples. However, the purpose of the examples is to illustrate the methodology and not to obtain accurate answers for a specific configuration. In addition, even with the non-linear C_m vs. α behavior for ARW-2, the methodology in this paper still predicts representative answers for ARW-2. To illustrate this, the appendix compares time histories, as predicted by the present methodology, with time histories which take the nonlinear behavior into account.

Example 1 - Elevon Deflection for Trim

Equation (5) is the expression for computing the elevon deflection required to trim a vehicle in 1g straight-and-level flight and is repeated here

$$\delta_{trim} = \frac{(h_n - h)C_{L_{trim}} - C_{m_o}}{\frac{\partial C_{m_o}}{\partial \delta}}$$

In this equation, the static margin, $(h_n - h)$, appears explicitly and the remainder of the terms in the equation are independent of static margin.

Using the appropriate data from Table II, equation (5) was used to compute δ_{trim} as a function of static margin for each of the 5 flight conditions. The solid lines in figures 4(a) and 4(b) are plots of δ_{trim} vs. static margin. For interest, the elevon deflections for trim were computed for static margins ranging from +15% (stable) to -15% (the static margin of primary interest in this study). The three curves in figure 4(a) correspond to flight conditions 1, 2, and 3 (varying dynamic pressure at constant Mach number); the three curves in figure 4(b) correspond to flight conditions 4, 5, and 2 (varying Mach number at constant dynamic pressure). The maximum allowable positive deflection of the elevons is shown by the heavy dashed line at 7°. The maximum allowable negative deflection (at -12°) is off scale and was never a factor in the analysis.

At each flight condition, the amount of elevon deflection required to trim the vehicle in 1g straight-and-level flight at -15% static margin is within the current available limits. From figure 4, the flight condition characterized by the lowest dynamic pressure (flight condition 1, or the "cruise condition") requires the largest amount of elevon deflection to trim the vehicle. In addition, the magnitude of the additional elevon deflection required to trim the vehicle at -15% (compared to +15%) is highest at the lowest dynamic pressure.

Example 2 - Steady-State Elevon Deflection for Pull-up Maneuver

Equation (9) is the expression for computing the steady-state elevon deflection required to trim a vehicle in a steady pull-up maneuver of incremental load factor n-1. Equation (9) is repeated here.

$$\Delta\delta = (n-1)\frac{(h_n-h)\left(C_{L_{trim}} - C_{L_q}\frac{\bar{c}g}{2V^2}\right) - C_{m_q}\frac{\bar{c}g}{2V^2}}{\frac{\partial C_{m_o}}{\partial \delta}}$$

In this equation, the static margin appears both explicitly as the quantity (h_n-h), and implicitly in the C_{L_q} and C_{m_q} stability derivatives. Because no information was available on the variation of these two stability derivatives with center of gravity position (and therefore with static margin), and because this variation is a second-order effect, for the purpose of this example, it was assumed that C_{L_q} and C_{m_q} were constant over the range of static margins considered.

Using the appropriate data from Table II, equation (9) was used to compute $\Delta\delta$ for a 1.5g incremental pull up at the five flight conditions and for static margins ranging from +15% to -15%. The sum of $\Delta\delta$ and δ_{trim} (eq. (6)) is the total steady-state deflection required for a 2.5g pull up,and such sums are plotted as the dashed lines in figures 4(a) and 4(b). In general, $\Delta\delta$ (the difference between the dashed and solid lines--see arrow in figure 4(a), top) is negative for positive static margin and positive for negative static margin, indicating that, to achieve the same pull-up maneuver, the elevon must deflect in the opposite sense (from a "conventional" deflection) when the airplane is statically unstable.

Referring again to the dashed lines in figures 4(a) and 4(b), these results indicate that, at each flight condition, the amount of steady-state elevon deflection required to trim the vehicle in a 2.5g pull-up maneuver at -15% static margin is within the current available limits. As was the case for Example 1, the flight condition with the lowest dynamic pressure requires the largest amount of elevon deflection to perform the maneuver.

Table V summarizes the results of Examples 1 and 2 for the condition of -15% static margin.

Example 3 - Time-Varying Elevon Deflection for Pull-up Maneuver

This example is based on equations (12) and (13) and follows the procedure outlined following equation (13). Because of limited information available, this example involves only the "cruise" flight condition and the two extreme values of static margin (+15% and -15%). Table III contains the numerical data used for this example.

The simplified but representative RSS active control system, whose block diagram appears in figure 5, is used in this example. It features angle-of-attack and pitch-rate feedback to the elevons. Referring back to the Methodology section, equation (10) contains the equations of motion for the "rigid airplane" box. The following equation represents the condition at the top summing junction in figure 5, and corresponds to equation (12) in the Methodology section

$$\Delta\delta = K_c\Delta\delta_{column} + K_\alpha\Delta\alpha + K_q\Delta q \tag{16}$$

Substituting equation (16) into equation (10) and rearranging yields the following equation in the time domain

$$\left.\begin{aligned}(2\mu t^*-C_{z_{\dot\alpha}}t^*)\Delta\dot\alpha - (C_{z_\alpha}+C_{z_\delta}K_\alpha)\Delta\alpha - (2\mu t^*+C_{z_q}t^*+C_{z_\delta}K_q)\Delta q = C_{z_\delta}K_c\Delta\delta_{column}\\ -C_{m_{\dot\alpha}}t^*\Delta\dot\alpha - (C_{m_\alpha}+C_{m_\delta}K_\alpha)\Delta\alpha + i_B t^{*2}\Delta\dot q - (C_{m_q}t^*+C_{m_\delta}K_q)\Delta q = C_{m_\delta}K_c\Delta\delta_{column}\end{aligned}\right\} \tag{17}$$

Equation (17) is analogous to equation (13) and represents the equations of motion of the entire block diagram in figure 5. The steps following equation (13) are performed to obtain the time-varying behavior of δ.

For the statically stable configuration (+15% static margin), it is assumed that gains K_α and K_q are zero, which, in effect, removes the feedback loops from the block diagram and forces $\Delta\delta$ to be proportional to δ_{column}. Gain K_c is -1.0, which means that pulling back on the column (positive) will produce a trailing-edge up deflection (negative) of the elevon. A "ramp-hold" $\Delta\delta_{column}$ forcing function is chosen which, when equation (17) is solved, results in a steady-state incremental pull-up of load factor 1.5 g's (eq. (11)). After solution of equation (17), the time history of incremental elevon deflection is available from equation (16). Using the trim elevon deflection at this flight condition for +15% static margin, the time history of total elevon deflection is available from equation (6). Time history plots of the column input, normal load factor, and total elevon deflection are presented in figure 6(a). The "ramp" portion of the input terminates at time 0.4 seconds, and thereafter the value of the input at 0.4 seconds is "held" for all remaining time. In response to the input, the time history of normal acceleration is seen to oscillate for several cycles (at the frequency of the short period mode of the vehicle). When the transients have died out, the vehicle is left in the condition of a steady-state 1.5g incremental (2.5g total) pull up.

The open and closed square symbols at the beginning and end (respectively) of the elevon deflection time history represent the steady-state values for 1g

straight-and-level flight and a 2.5g pull up (respectively). These symbols correspond to the square symbols on the top plot in figure 5(a), indicating that both the steady-state and time-varying analyses predict the same terminal values of $\Delta\delta$. The entire time history of elevon deflection in figure 6(a) is within the current available limits.

The next two sets of time histories are for the -15% static margin condition with the RSS active control system on. They differ from each other in the values of the feedback gains and in the magnitudes of the ramp-hold column input. Both sets result in a 2.5g steady-state pull-up maneuver. The initial and final values of elevon deflection for both sets are identical, and correspond to the open and closed circle symbols in figure 4(a). The initial and final values of elevon deflection are within the current available limits. (For the initially statically unstable configuration at -15% static margin--with feedback gains K_α and K_q equal to zero--the characteristic equation has two real roots: one negative and one positive. By proper choice of feedback gains K_α and K_q, these roots may be moved to any location in the complex plane. The "new" location of these roots may be referred to as the "augmented" short period mode.)

For the time histories in figure 6(b), gains K_α and K_q are chosen such that the roots of the "augmented" short period mode are identical to the actual roots of the short period made at +15% static margin. For the time histories in figure 6(c), K_α and K_q are chosen such that the "augmented" short period mode has the same damped natural frequency as the actual short period mode at +15% static margin, but has a damping ratio of 0.707. The value of K_c corresponding to figures 6(b) and 6(c) is again -1.0. Table VI presents the characteristic roots, the corresponding damping ratio and damped natural frequency, and RSS active control system gains for the three configuration represented in figures 6(a), 6(b), and 6(c).

In figures 6(b) and 6(c), even though the initial and final values of elevon deflection are the same and result in a 2.5g steady-state pull up in each case, the transient values of elevon deflection are very different. In figure 6(b), the transient elevon deflection required to perform the maneuver exceeds the maximum allowable trailing-edge-down deflection; in figure 6(c) the transient deflection is within the available limits. This comparison illustrates the fact that elevon deflections are very much dependent on the characteristics of the RSS active control system. To a certain degree, by proper choice of feedback gains, transient elevon deflections for a pull-up maneuver may be made to fall within the available limits. However, it should be noted that, in figure 6(c), the deflection being within available limits is at the expense of a nearly two-fold increase in the magnitude of $\Delta\delta_{column}$ to perform the same pull-up maneuver. A summary of key deflections for this example is also presented in Table VI.

Example 4 - Time-Varying Elevon Deflection for Roll Maneuver

The data from Table IV was used in this example. This example is based on equations (14) and (15), and, in addition, it is based on something (a complication) not mentioned in the Methodology section because the

complication is a characteristic of the ARW-2 configuration (and not necessarily true for all airplanes in general). This characteristic is that the ARW-2 configuration has an unstable Dutch Roll mode for many points within its flight envelope and for all 5 flight conditions considered in this paper. The Dutch Roll was not designed to be unstable nor is it a feature or consequence of any active control concept. However, it must be stabilized by use of a lateral-directional automatic flight control system (AFCS). The block diagram in figure 7 contains that portion of a lateral-directional AFCS (proposed for ARW-2) which applies to a roll maneuver. In order to perform this example, the following equations (which describe the two loops in figure 7) must be combined with equation (14) and (15)

$$\left.\begin{aligned} \Delta\delta_r &= \left(\frac{20}{S+20}\right)(K_1)\left(\frac{S}{S+2}\right)(\Delta\dot{\psi}+0.07\Delta\dot{\phi}) \\ \Delta\delta_d &= \left(\frac{20}{S+20}\right)(K_2)\left[\left(3.5+\frac{1}{S}\right)\Delta\delta_{wheel}+\frac{1}{S}\Delta\dot{\phi}\right] \end{aligned}\right\} \qquad (18)$$

Because of the necessity of including equation (18) in this example, the procedure for assessing the roll maneuver (originally discussed after equation (15) in the Methodology section) must be altered. For this example, the time-varying behavior of roll angle, $\Delta\phi$, and differential elevon deflection, $\Delta\delta_d$, are found by the following steps:

Step 1: Combine and re-write equations (15) and (18) so that $\Delta\delta_r$ and $\Delta\delta_d$ are eliminated from the equations and $\Delta\delta_{wheel}$ appears as the forcing function on the right-hand side of the new equations.

Step 2: Input a unit ramp-hold function (ramp terminating at 0.4 seconds) for $\Delta\delta_{wheel}$ and solve the new equations for responses $\Delta\beta$, Δp, Δr, $\Delta\phi$, $\Delta\psi$, and their derivatives.

Step 3: Because these equations are linear equations, scale the input, the responses, and their derivatives by the amount required for the value of roll angle to be exactly 30° at time 3 seconds.

Step 4: Using these scaled quantities in equation (18), compute the value of differential elevon deflection.

Step 5: Make use of equation (14) (with the value of δ_{trim} corresponding to -15% static margin) to compute the total right and left elevon deflections.

The values of elevon deflection computed in this manner are the minimum deflections necessary to perform the MIL SPEC roll maneuver. Such deflections may then be compared with the maximum allowable deflections on the vehicle.

Figure 8 contains time histories (computed according to this procedure) of ramp-hold wheel input, roll angle, and total right and left elevon deflections at the cruise condition. The value of roll angle is seen to be 30° at time 3 seconds. Because of the dynamics associated with the AFCS, the time history of elevon deflection peaks at a time of about 0.8 seconds. The elevon deflection for performing the MIL SPEC roll maneuver is well within the available limits.

Similar calculations were made (with similar results) at the other four flight conditions. The time histories are substantially the same at each flight condition (with the major difference being the magnitudes of the responses) and all elevon deflections are well within the available limits. These remaining time histories are not presented, but the results at all five flight conditions are summarized in Table VII. As seen in a previous example, the flight condition with the lowest dynamic pressure (the one depicted in fig. 8) requires the largest amount of elevon deflection to perform the maneuver.

CONCLUDING REMARKS

This paper presents both the methodology for computing elevon deflections required to trim and maneuver a vehicle with -15% static margin and an application of the methodology. The methodology is based on linear analyses of the rigid-body dynamics of a vehicle with a relaxed-static-stability (RSS) active control system. The longitudinal and lateral-directional equations are uncoupled.

The methodology is presented to provide a means for answering the question: Can the Firebee II drone vehicle, with its standard elevons, but fitted with a new reseach wing and a new active control system, be trimmed and maneuvered with a static margin of -15%? The characteristics of the new wing and active control system are not yet known, so that this question cannot now be answered. However, by applying the methodology to the ARW-2 wing (which has many similar features--supercritical airfoil, low sweep, high aspect ratio--to a class of possible new wings) with a simplified (but representative of a new) RSS active control system, an initial attempt to address this question has been made. On the basis of performing analyses at 5 representative flight conditions, it appears possible to trim and maneuver the vehicle with -15% static margin with the existing elevons. The results of these examples indicate that transient elevon deflections depend heavily on the characteristics of the active control system.

APPENDIX

COMPARISON OF RESULTS: PRESENT METHODOLOGY VS. NONLINEAR SIMULATION

The purpose of this appendix is to present the results of another application of the methodology of this paper. The particular application is the ARW-2 configuration with its intended active control system (consisting, in this case, of an automatic flight control system--AFCS--and a relaxed static stability--RSS--system). This example will provide an indication of the suitability of the present methodology (which is based on the assumption of linear vehicle aerodynamic characteristics) to a vehicle which has very nonlinear aerodynamic characteristics. Time histories (for pull-up only) computed using this methodology will be compared to time histories obtained from a "nonlinear simulation" (an analysis which takes the nonlinear aerodynamic characteristics into account and which, therefore, more accurately describes the actual vehicle in flight).

Flight Condition

The flight condition for this application is Mach number of 0.7, dynamic pressure of 19.60 kPa (409.3 psf), altitude of 4572 m (15 000 ft), and is identified as point 6 in Table I and figure 3.

Aerodynamic Characteristics

Figure 9 contains the plots of ARW-2 lift and moment coefficients as functions of angle of attack for this flight condition. These characteristics are seen to be very nonlinear, and they are represented in this manner in the nonlinear simulation. The dashed lines in figure 9 represent "instantaneous" slopes of these curves (C_{L_α} and C_{m_α}, respectively) at an average angle of attack (see the Results section for further discussion of this). The zero-lift pitching moment, $C_{m_{0_0}}$, identified in figure 9 is the value which would result if the pitching moment were linear with angle of attack and had the slope it has at the average value of angle of attack.

Table VIII contains the data necessary to perform the calculations for δ_{trim} and $\Delta\delta$ using equations (5) and (9), respectively. The value of static margin, (h_n-h), indicated for table VIII was obtained by using the instantaneous values of C_{L_α} and C_{m_α} and the relation $C_{L_\alpha} = C_{m_\alpha}(h-h_n)$. Table IX contains the data necessary to describe the airplane for the time-varying pull-up analysis. The information in figure 9 and Tables VIII and IX was obtained from a third unpublished document on the ARW-2 configuration.

Active Control System

Figure 10 contains the block diagram of the AFCS and RSS for the ARW-2 vehicle with the appropriate gains for this flight condition.

Results

For convenience, the time-varying analysis for pull-up maneuver will be discussed first. Discussion of steady-state results (for δ_{trim} and $\Delta\delta$) will follow.

Time-varying analysis.- Figure 11 contains time histories of column input ($\Delta\delta_{column}$), and responses normal acceleration (Δn), pitch rate (Δq), angle of attack (α), and elevon deflection (δ). The solid curves are the responses which were obtained from the methodology of this paper; the dashed curves are those from the nonlinear simulation. The input is a ramp-hold column deflection with the break at 0.4 seconds and magnitude 1.32. This input was used for both analyses. For the case of the nonlinear simulation this input produced a steady-state incremental normal acceleration of 1.5 g's.

To obtain the time histories using the present methodolgy, constant values of C_{L_α} and C_{m_α} had to be obtained from figure 9. Such values were obtained in the following manner: (1) from the α time history in figure 11, determining the average value of angle of attack for the dashed curve between the initiation and the completion of the maneuver and (2) from figure 9, determining the "instantaneous" values of C_{L_α} and C_{m_α} at the angle of attack obtained from (1).

In comparing the time histories in figure 11, all responses compared favorably in terms of magnitude and general character of response. With the exception of angle of attack, all reponse values (at time 4 seconds) for the present methodology are within about 10% of their respective values (at the same time) for the nonlinear simulation. (The difference in steady state angle-of-attack responses is due, in large part, to the inclusion of the speed degree of freedom--phugoid mode--in the nonlinear simulation. Reduction in forward speed--not shown--occurs in response to the input. This decrease in speed causes a reduction in dynamic pressure which then necessitates a larger angle of attack to perform the required maneuver.) The time histories from the present methodology are seen to be more lowly damped and have a slightly higher frequency of oscillation within the transient than those from the nonlinear simulation.

The steady-state elevon deflection angle, as predicted by the present methodology, is within one-quarter of a degree of that predicted by the nonlinear simulation. In addition, even for the maximum and minimum peaks of the solid elevon time history, the response is well within the available limits and only exceeds the minimum and maximum values of the dashed curve by -0.3° and 0.1°, respectively. In terms of a simple (linear) analytical method for estimating quantities for a very nonlinear system, the present methodology appears to be suitable.

Steady-state analysis.- Equations (5), (6), and (9) were used with the data from table VIII to calculate quantities δ_{trim}, $\Delta\delta$, and δ_n. This discussion will begin by referring back to figure 11 to bring out the following point: the incremental normal acceleration for the present methodology at time 4 seconds (essentially steady state) is 1.38 g's. Therefore, 1.38 was used for the quantity (n-1) in equation (9). The row labelled "present

methodology" in Table X contains the results of applying equations (5), (6), and (9) to the data from Table VIII. The quantities in the row labelled "nonlinear simulation" were obtained directly from the time response in figure 11. The comparison of the results from the two analyses indicates differences no greater than 13% on a relative basis, or one-quarter of a degree on an absolute basis.

The quantities δ_{trim} and δ_n from the "present methodology" row of Table X are plotted as the open and closed diamond symbols in figure 11. This again illustrates a point made in the main body of the paper: that the steady state value of elevon deflection is independent of the characteristics of the active control system.

REFERENCES

1. Schoenman, R. L.; and Shomber, H. A.: Impact of Active Controls on Future Transport Design, Performance, and Operation. SAE Paper No. 751051, November, 1975.

2. Anon.: Flying Qualities of Piloted Airplanes. Military Specification MIL-F-8785B (ASG), August, 1969.

3. Etkin, Bernard: Dynamics of Flight. John Wiley and Sons, Inc., New York, 1959.

TABLE I.- FLIGHT CONDITIONS.

Condition (see fig. 3)	Mach Number	Dynamic Pressure		Altitude	
		kPa	psf	m	ft
1	0.8	6.071	126.8	14,265	46,800
2	.8	12.14	253.6	9,815	32,200
3	.8	24.28	507.2	4,968	16,300
4	.6	12.14	253.6	5,852	19,200
5	.7	12.14	253.6	8,047	26,400
6	.7	19.60	409.3	4,572	15,000

TABLE II.- DATA USED TO PERFORM ANALYSES FOR NUMERICAL EXAMPLES 1 AND 2.

Quantity	Value of quantity at flight condition -				
	1	2	3	4	5
$C_{L_{trim}}$ [a]	0.5295	0.2648	0.1324	0.2648	0.2648
$C_{m_{o_o}}$	.0604	.0739	.1013	.0645	.0709
$\frac{\partial C_{m_o}}{\partial \delta}$	-2.781	-2.805	-2.859	-2.395	-2.520
$\bar{c}$(m)	.596	.596	.596	.596	.596
V(m/sec)	236.7	240.0	256.4	190.2	215.4
C_{L_q}	6.40	5.85	5.00	5.70	5.75
C_{m_q}	-32.1	-32.0	-31.7	-29.0	-30.3

[a] Based on vehicle weight of 10453 N (2350 lb)

TABLE III.- DATA USED TO PERFORM ANALYSIS FOR NUMERICAL EXAMPLE 3.

Quantity	Value of quantity for static margin of -	
	+15%	-15%
t^*(sec)	0.00126	0.00126
μ [a]	5,081	5,081
i_B [b]	182,896	182,896
C_{Z_α}	-8.638	-8.638
$C_{Z_{\dot{\alpha}}}$	-2.76	-2.76
C_{Z_q}	-6.40	-6.40
C_{Z_δ}	-.848	-.848
C_{m_α}	-1.296	+1.296
$C_{m_{\dot{\alpha}}}$	-10.62	-10.62
C_{m_q}	-32.1	-32.1
C_{m_δ}	-2.908	-2.654

[a] Based on vehicle weight of 10453 N (2350 lb)

[b] Based on vehicle pitch moment of inertia of 3410 kg-m^2 (2515 slug-ft^2)

TABLE IV.- DATA USED TO PERFORM ANALYSIS FOR NUMERICAL EXAMPLE 4

Quantity	Value of Quantity at Flight Condition -				
	1	2	3	4	5
t^* (sec)	.0122	.0124	.0132	.0098	.0111
μ^a	523.4	268.7	153.4	168.7	216.6
$i_A{}^b$	18.92	9.71	5.55	6.10	7.83
$i_C{}^c$	253.8	130.3	74.4	81.8	105.0
$i_E{}^d$	5.446	2.796	1.596	1.755	2.254
$C_{L_{trim}}^a$	.5295	.2648	.1324	.2648	.2648
C_{y_β}	-1.09	-1.09	-1.09	-1.09	-1.03
C_{y_p}	-.15	-.15	-.15	-.15	-.15
C_{y_r}	.615	.615	.615	.570	.590
$C_{y_{\delta_d}}$	0	0	0	0	0
$C_{y_{\delta_r}}$	.119	.119	.119	.119	.119
C_{ℓ_β}	-.132	-.166	-.155	-.149	-.149
C_{ℓ_p}	-.633	-.541	-.405	-.495	-.514
C_{ℓ_r}	.0945	.0670	.0430	.0660	.0670
$C_{\ell_{\delta_J}}$	-.0172	-.0172	-.0172	-.0164	-.0167
$C_{\ell_{\delta_r}}$	.0190	.0190	.0190	.0099	.0105
C_{n_β}	.022	.016	.019	.012	.013
C_{n_p}	-.0095	.0045	.0230	.0070	.0060
C_{n_r}	-.234	-.234	-.234	-.213	-.222
$C_{n_{\delta_d}}$	-.0116	-.0116	-.0116	-.0109	-.0116
$C_{n_{\delta_r}}$	-.044	-.044	-.044	-.044	-.044

a Based on vehicle weight of 10453 N (2350 lbs.)

b Based on vehicle roll moment of inertia of 322.7 kg-m^2 (233 slug-ft^2)

c Based on vehicle yaw moment of inertia of 4328 kg-m^2 (3192 slug-ft^2)

d Based on vehicle roll-yaw product of inertia of 92.9 kg-m^2 (68.5 slug-ft^2)

TABLE V.- SUMMARY OF ELEVON DEFLECTIONS FOR EXAMPLES 1 AND 2.

(Static margin = -15%)

Flight Condition	δ_{trim} (deg)	$\Delta\delta$ (deg)	$\delta_{2.5g}$ (deg)
1	2.88	2.40	5.28
2	2.32	1.17	3.49
3	2.43	0.55	2.98
4	2.49	1.34	3.83
5	2.52	1.29	3.81

TABLE VI.- SUMMARY OF INFORMATION FOR EXAMPLE 3.

Static Margin	RSS System Gains			Characteristic Roots (rad/sec)	ζ	ω_d (rad/sec)	δ_{column} (deg)	δ_{trim} (deg)	δ_{peak} (deg)	$\delta_{2.5g}$ (deg)
	K_c	K_α	K_q							
+15%	-1.	0.	0.	-.431 ± i 2.09	.202	2.09	2.51	-.39	-2.90	-2.90
-15%	-1.	.982	-.007	-.431 ± i 2.09	.202	2.09	2.51	2.88	7.79	5.28
-15%	-1.	1.18	.355	-2.09 ± i 2.09	.707	2.09	4.80	2.88	5.77	5.28

TABLE VII.- SUMMARY OF INFORMATION FOR EXAMPLE 4

(-15% Static Margin)

Flight Condition	ϕ At Time 3 Seconds	δ_{wheel} (deg)	δ_{trim} (deg)	Maximum Deflections			K_1	K_2
				δ_d (deg)	δ_L (deg)	δ_R (deg)		
1	30	8.27	2.88	2.28	0.60	5.16	2.06	.149
2	30	8.66	2.32	1.21	1.11	3.53	1.03	.075
3	30	8.67	2.43	0.61	1.82	3.04	.515	.037
4	30	10.2	2.49	1.46	1.03	3.95	1.03	.075
5	30	9.07	2.52	1.28	1.24	3.80	1.03	.075

TABLE VIII.- DATA NECESSARY TO PERFORM CALCULATIONS FOR δ_{trim} AND $\Delta\delta$

(Static Margin = -6.19%)

Quantity	Value of Quantity
$C^{a}_{L_{trim}}$	.164
$C_{m_{o_o}}$	.070
$\frac{\partial C_{m_o}}{\partial \delta}$	-2.61
$\bar{c}$ (m)	.596
V (m/sec)	225.5
C_{L_q}	5.30
C_{m_q}	-30.1

[a] Based on vehicle weight of 10453 N (2350 lbs.)

TABLE IX.- DATA NECESSARY TO PERFORM CALCULATIONS FOR TIME-VARYING PULLUP

(Static Margin = -6.19%)

Quantity	Value of Quantity
t^* (sec)	.00132
μ [a]	1426
i_B [b]	44380
C_{z_α}	-5.529
$C_{z_{\dot{\alpha}}}$	-1.45
C_{z_q}	-5.30
C_{z_δ}	-.814
C_{m_α}	+.342
$C_{m_{\dot{\alpha}}}$	-5.52
C_{m_q}	-30.1
C_{m_δ}	-2.56

[a] Based on vehicle weight of 10453 N (2350 lbs.)

[b] Based on vehicle pitch moment of inertia of 2947 kg-m^2 (2173 slug-ft^2)

TABLE X.- SUMMARY OF ELEVON DEFLECTIONS FOR PRESENT METHODOLOGY AND NONLINEAR SIMULATION

Type Analysis	δ_{trim} (deg)	$\Delta\delta$ (deg)	δ_n (deg)
Present Methodology	1.76	0.25[a]	2.01[a]
Nonlinear Simulation	2.00	0.23[b]	2.23[b]

[a] Based on 1.38 g (incremental) pull up

[b] Based on 1.50 g (incremental) pull up

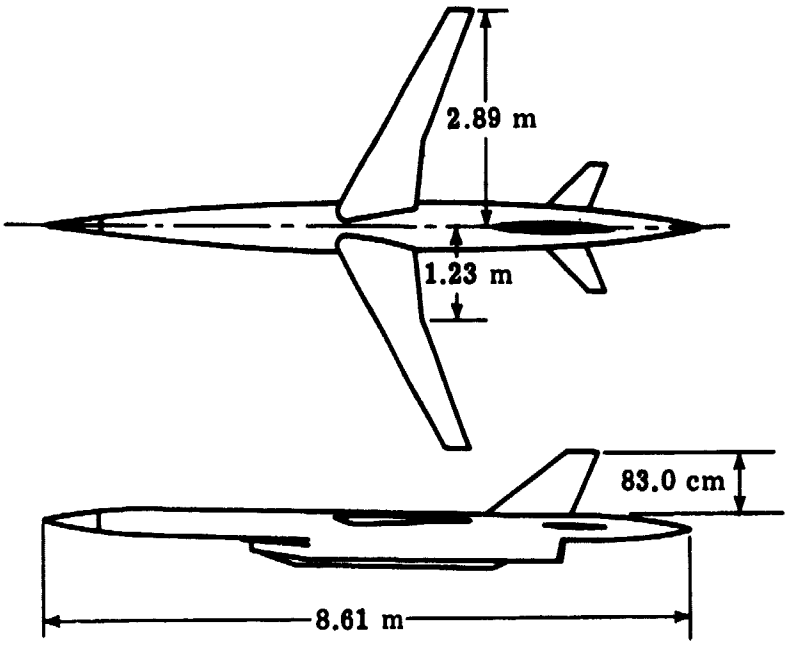

(a) DAST vehicle with ARW-2 wing.

Elevon geometry	
Gross area	0.836 m^2
Net exposed area	0.511 m^2
Aspect ratio	3.5
Taper ratio	0.4
Dihedral	0^o
Incidence	All-moving
Max deflections	7^o T.E. down 12^o T.E. up

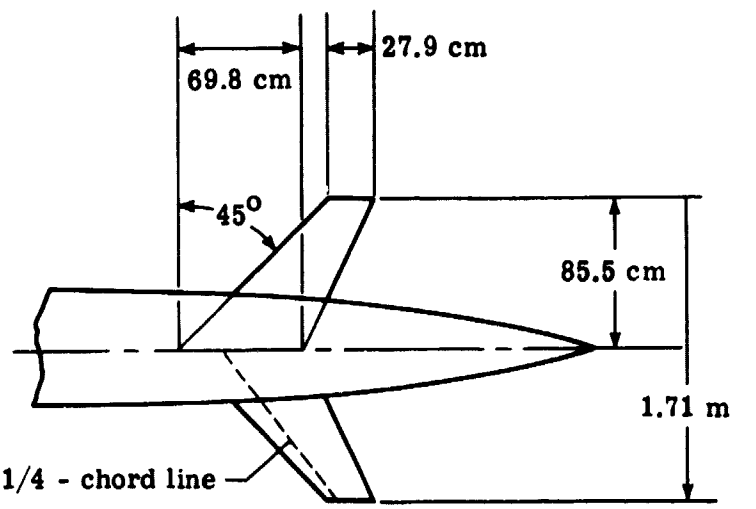

(b) Detail of elevon.

Figure 1.- DAST vehicle and elevon.

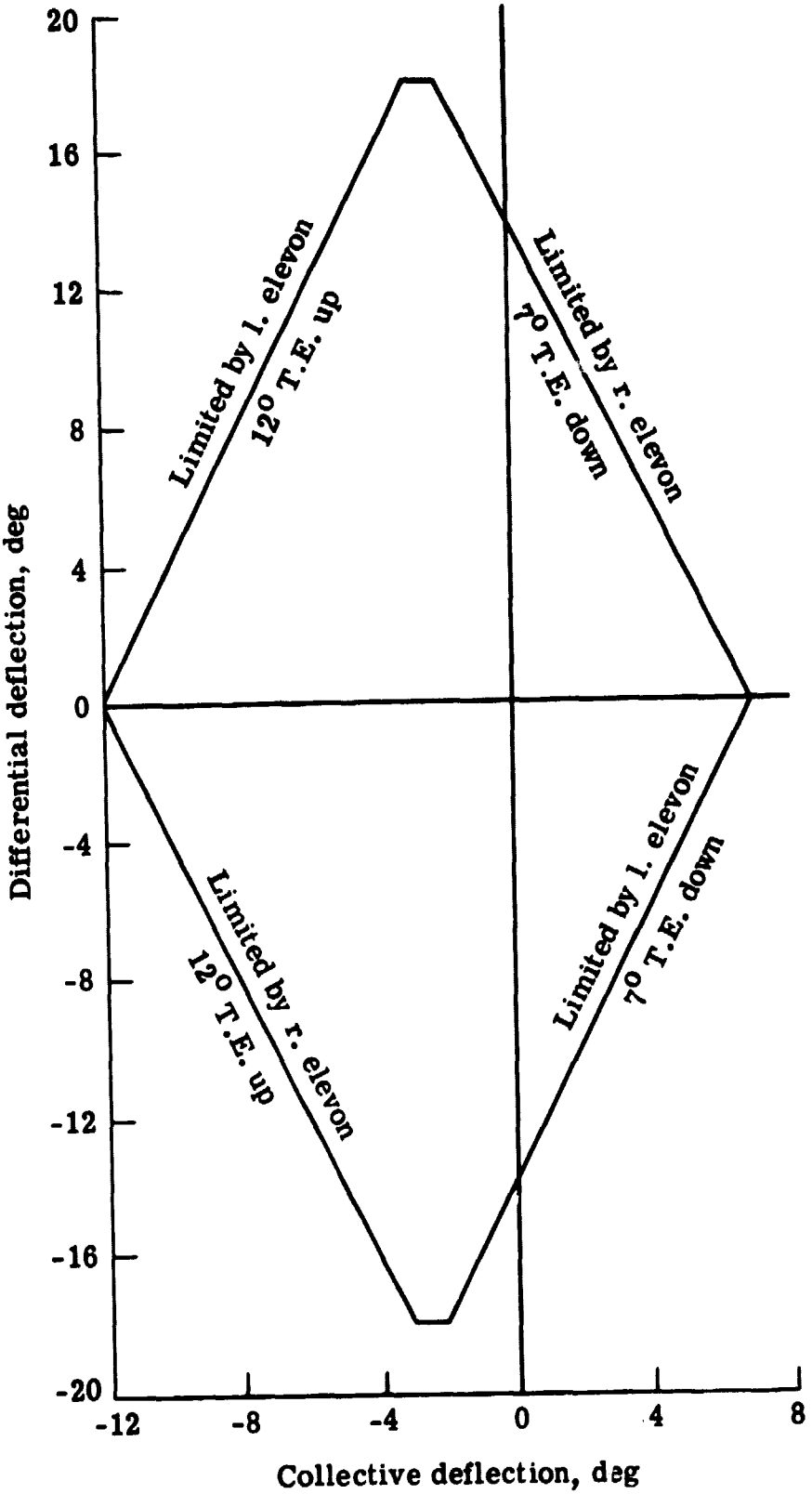

Figure 2.- Envelope of maximum available limits for elevon deflection.

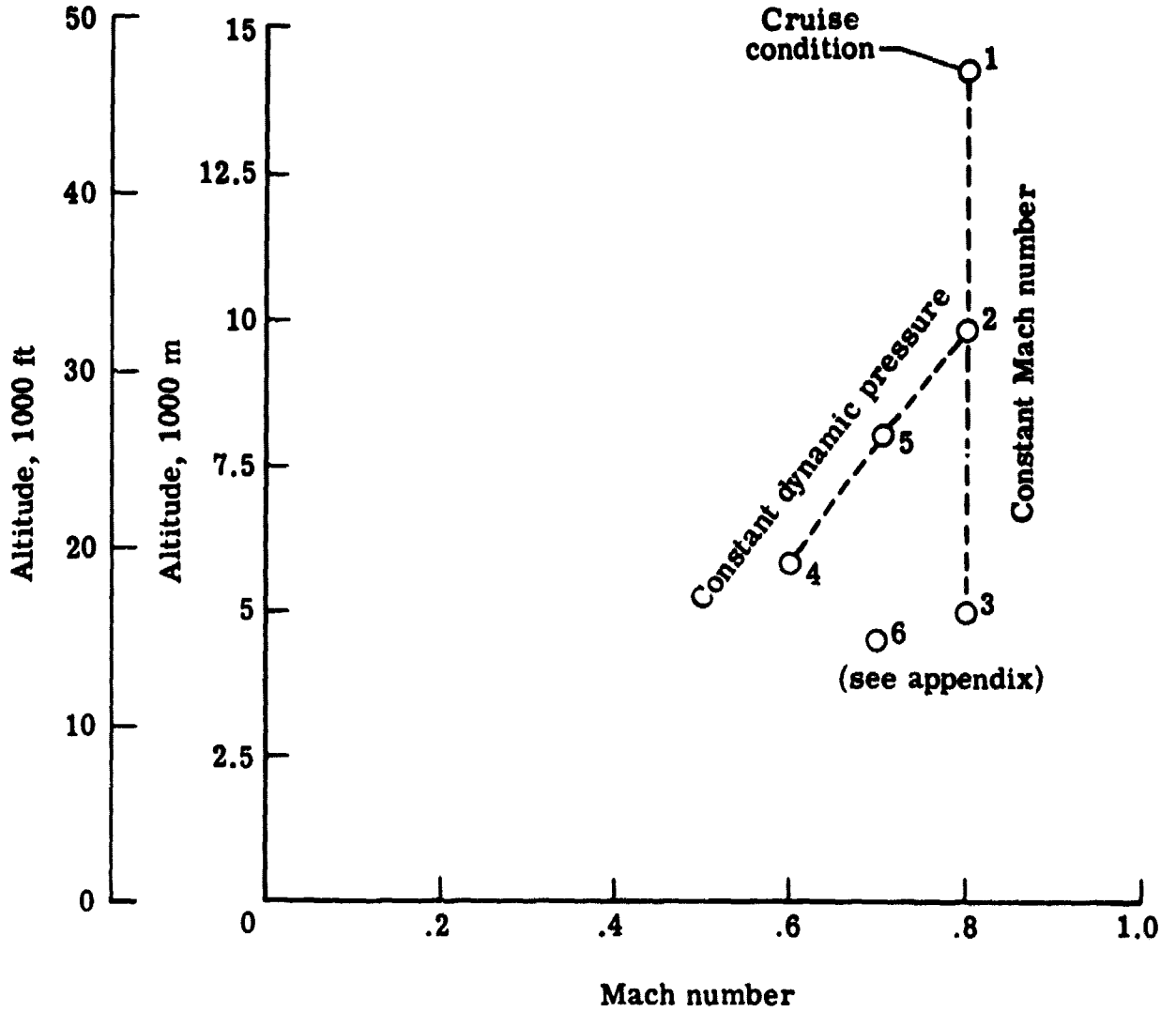

Figure 3.- Flight conditions for numerical examples.

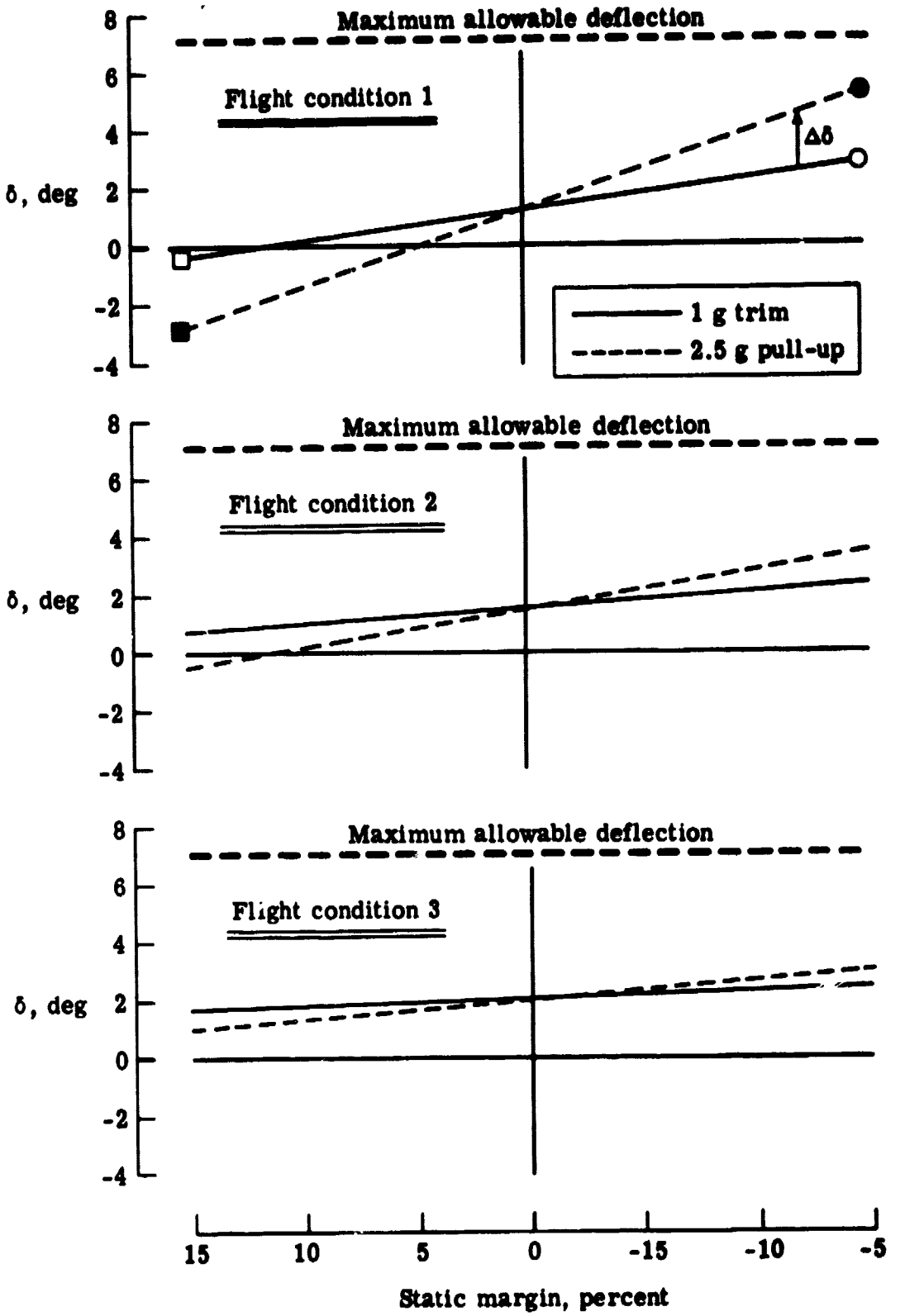

(a) M = 0.8

Figure 4.- Elevon deflections for trim and pull-up as a function of static margin.

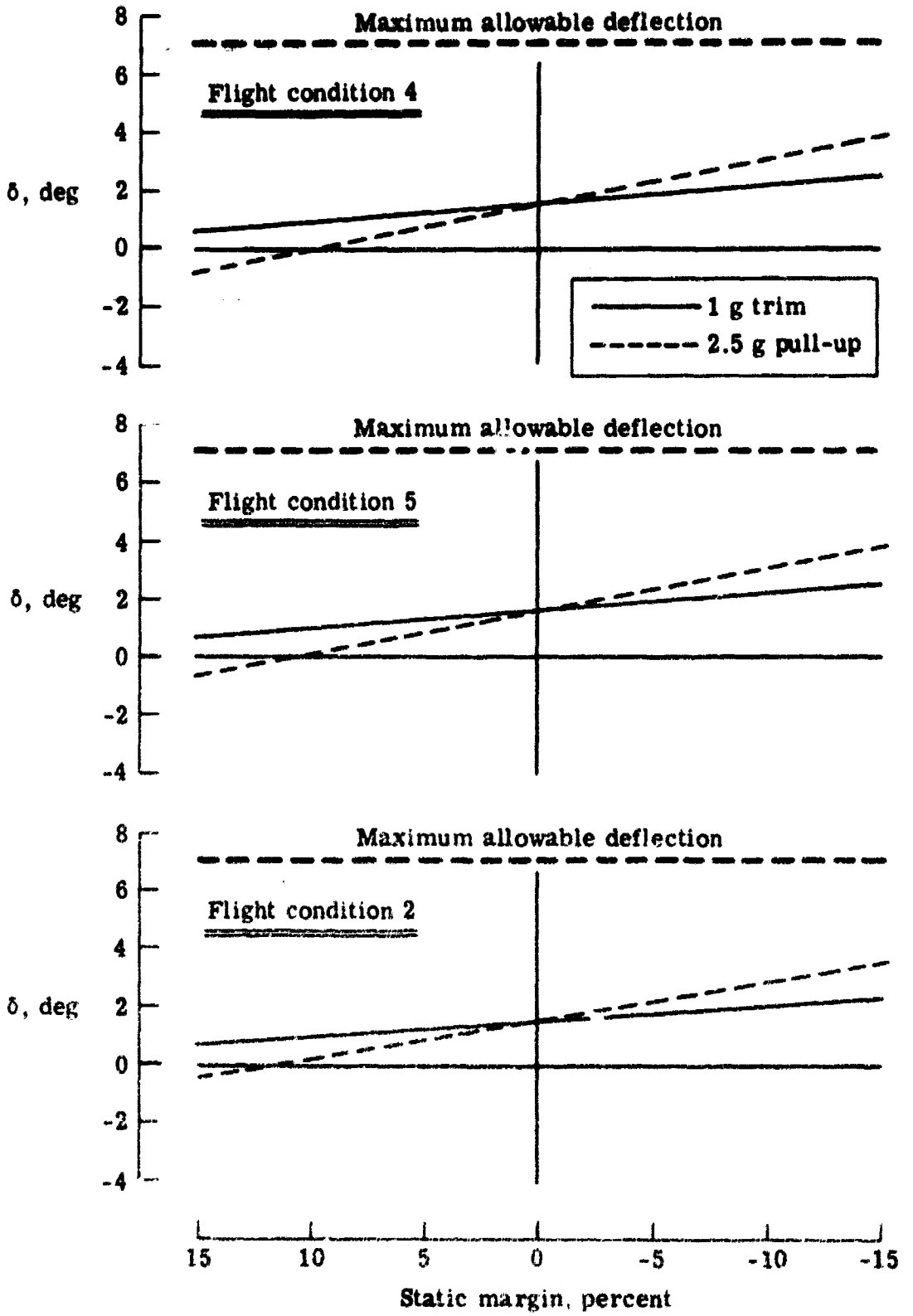

(b) q = 12.14 kPa

Figure 4.- Concluded.

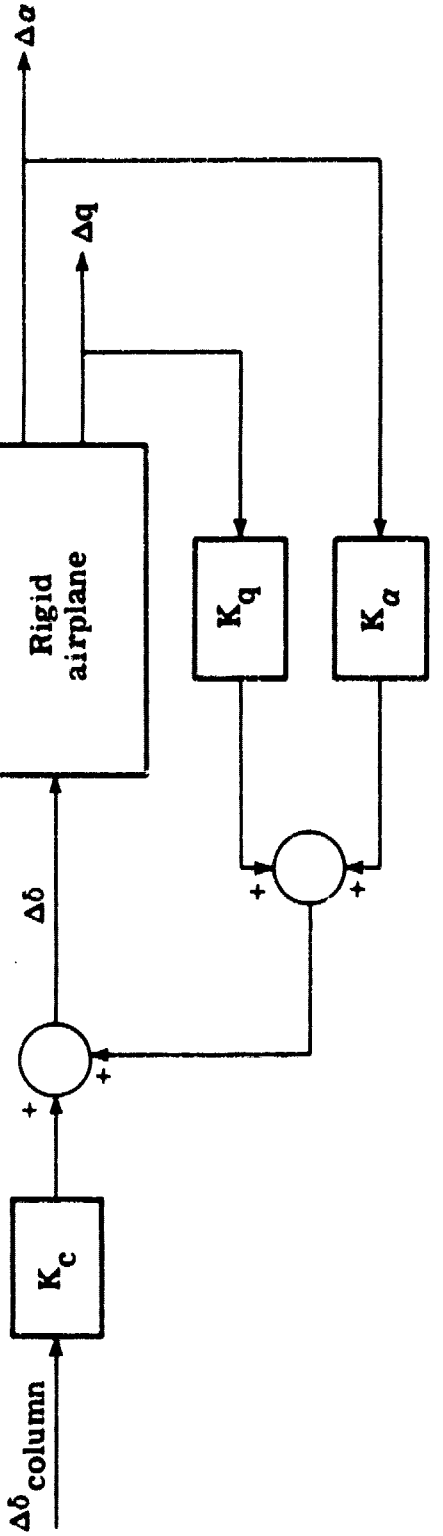

Figure 5.- Simplified RSS active control system.

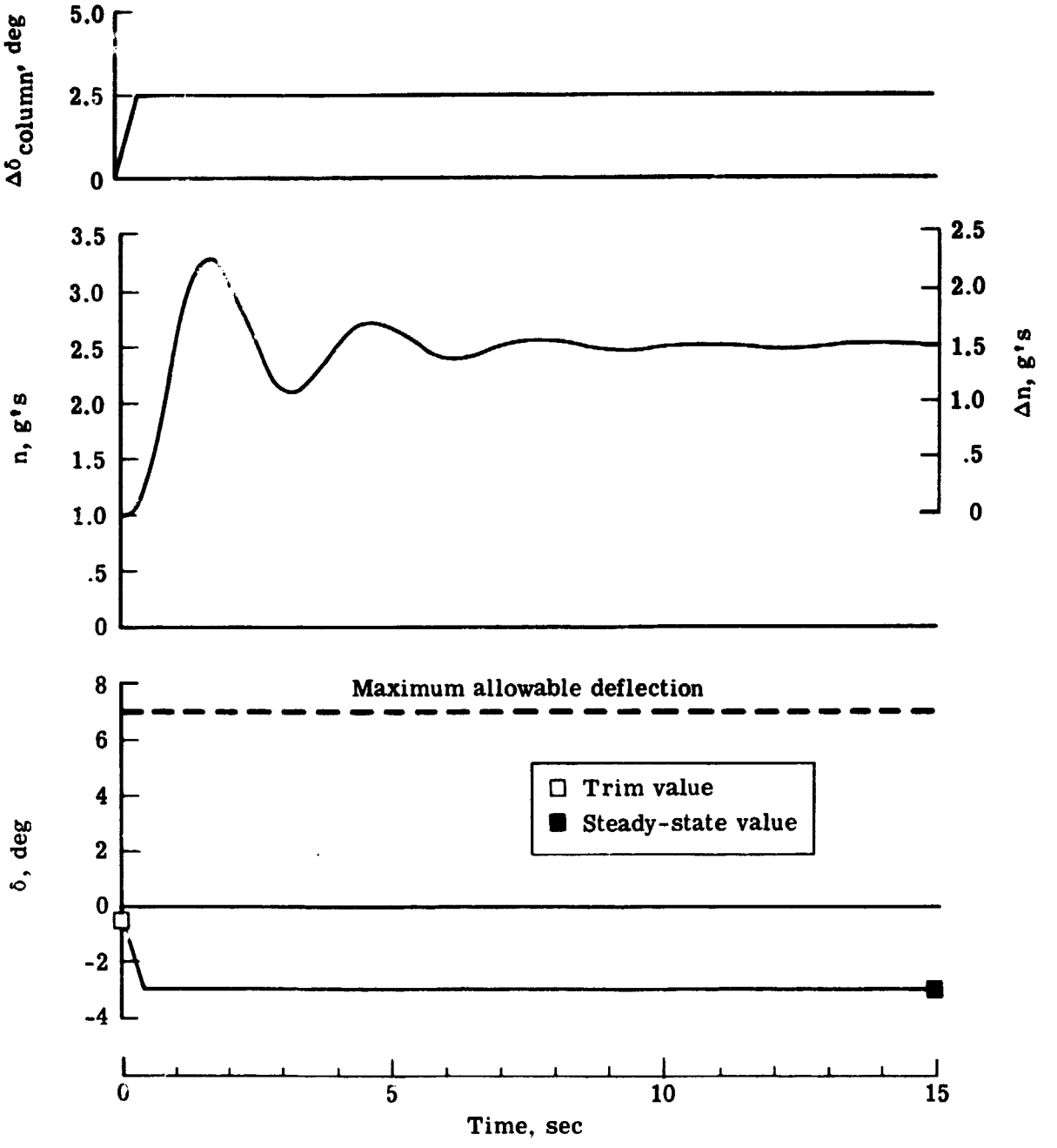

(a) +15% static margin; $K_\alpha = 0$, $K_q = 0$.

Figure 6.- Time histories for pull-up manuver.
Flight condition 1.

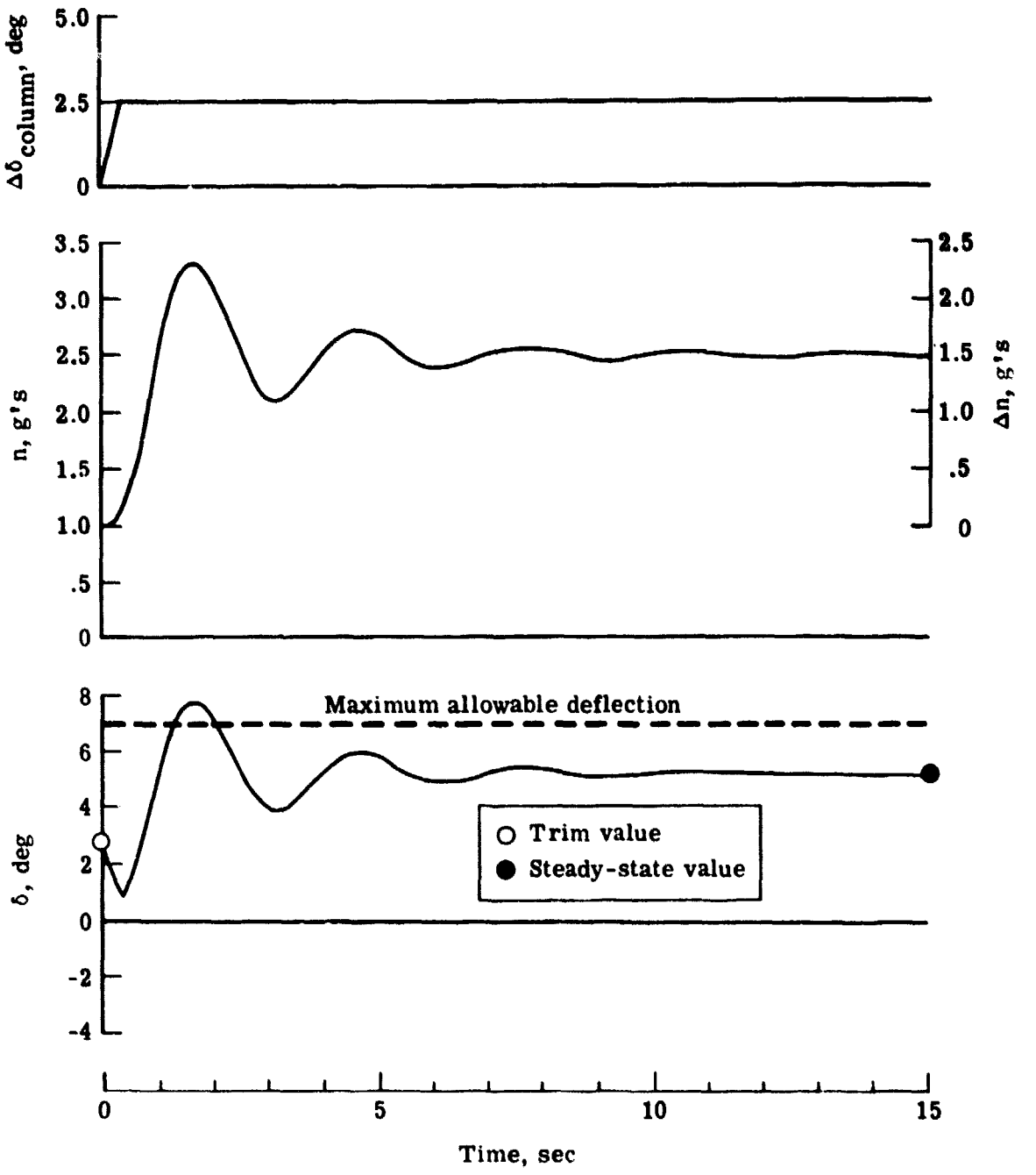

(b) - 15% static margin; K_α = 0.982, K_q = -0.007

Figure 6.- Continued.

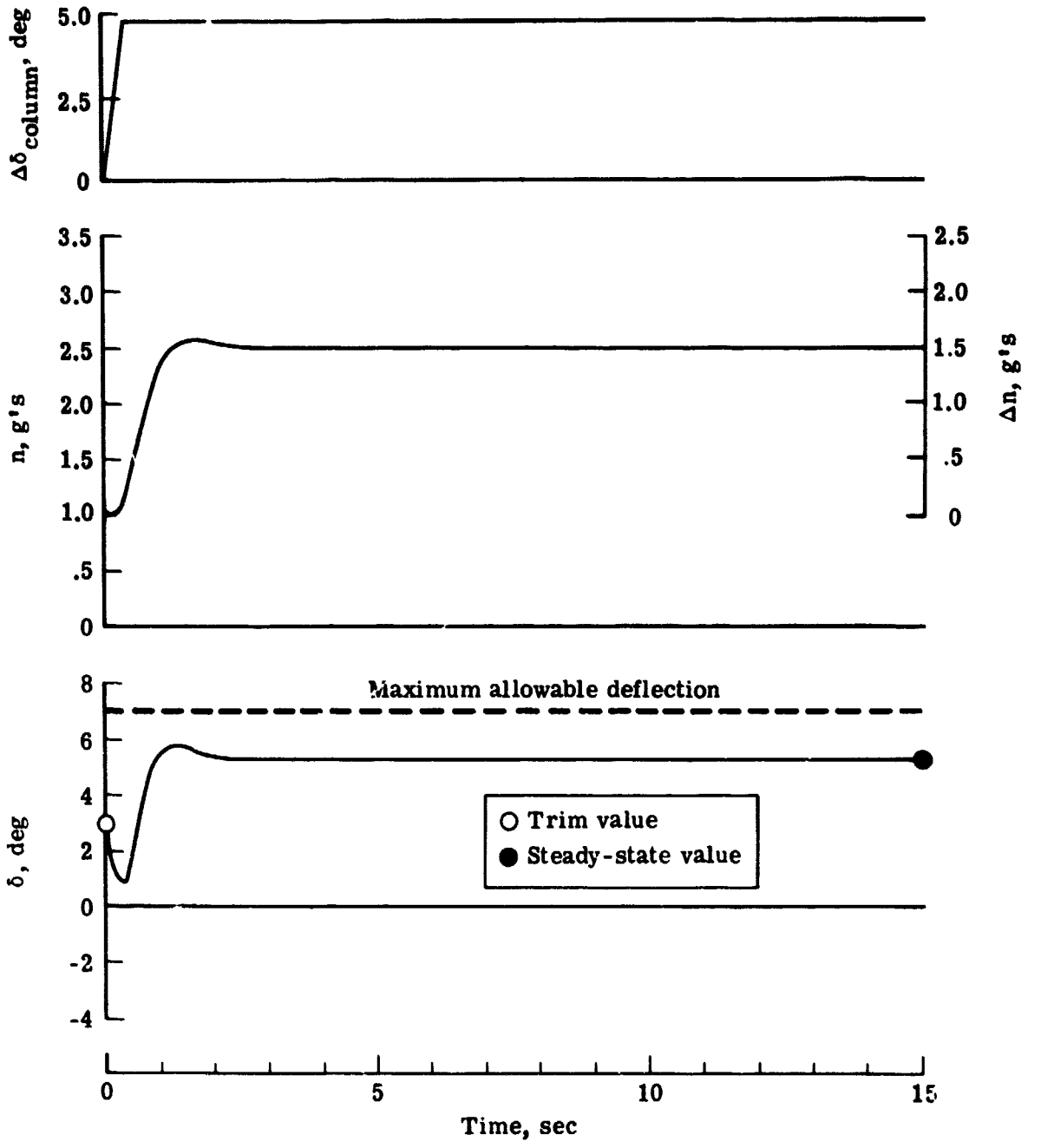

(c) - 15% static margin; K_α = 1.18, K_q = 0.355

Figure 6.- Concluded.

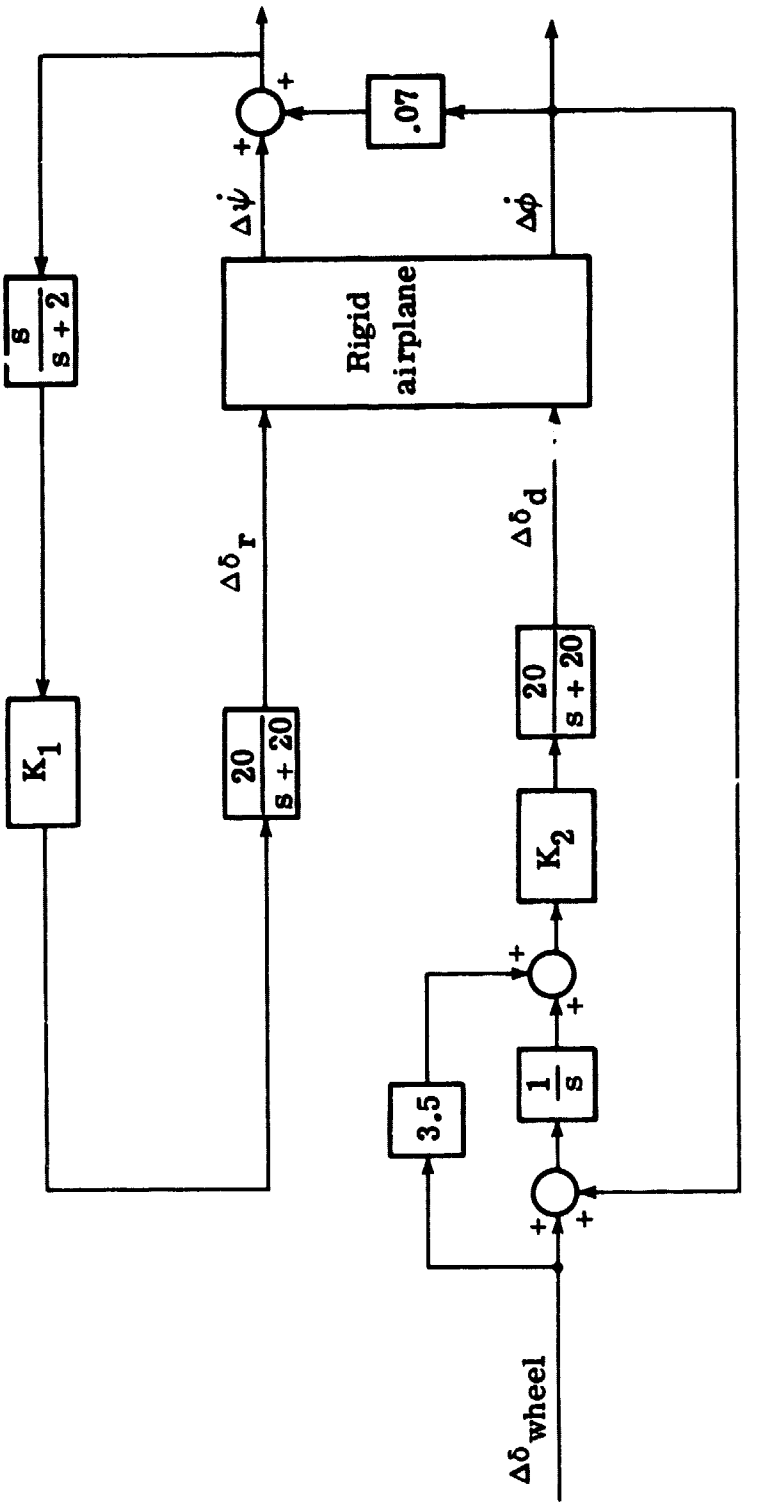

Figure 7.- Lateral-directional automatic flight control system.

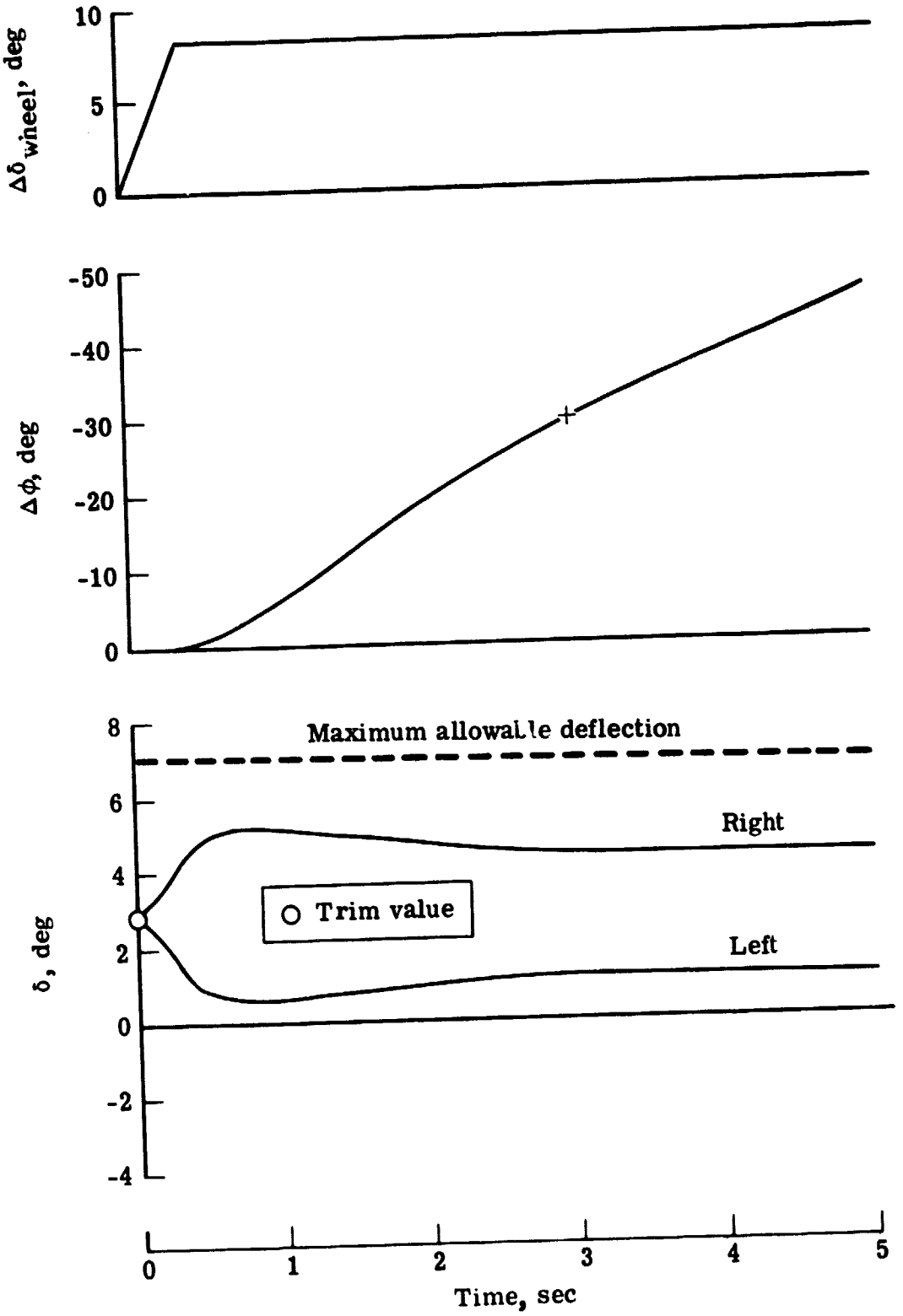

Figure 8.- Time histories for roll manuver. 15% static margin. Flight condition 1.

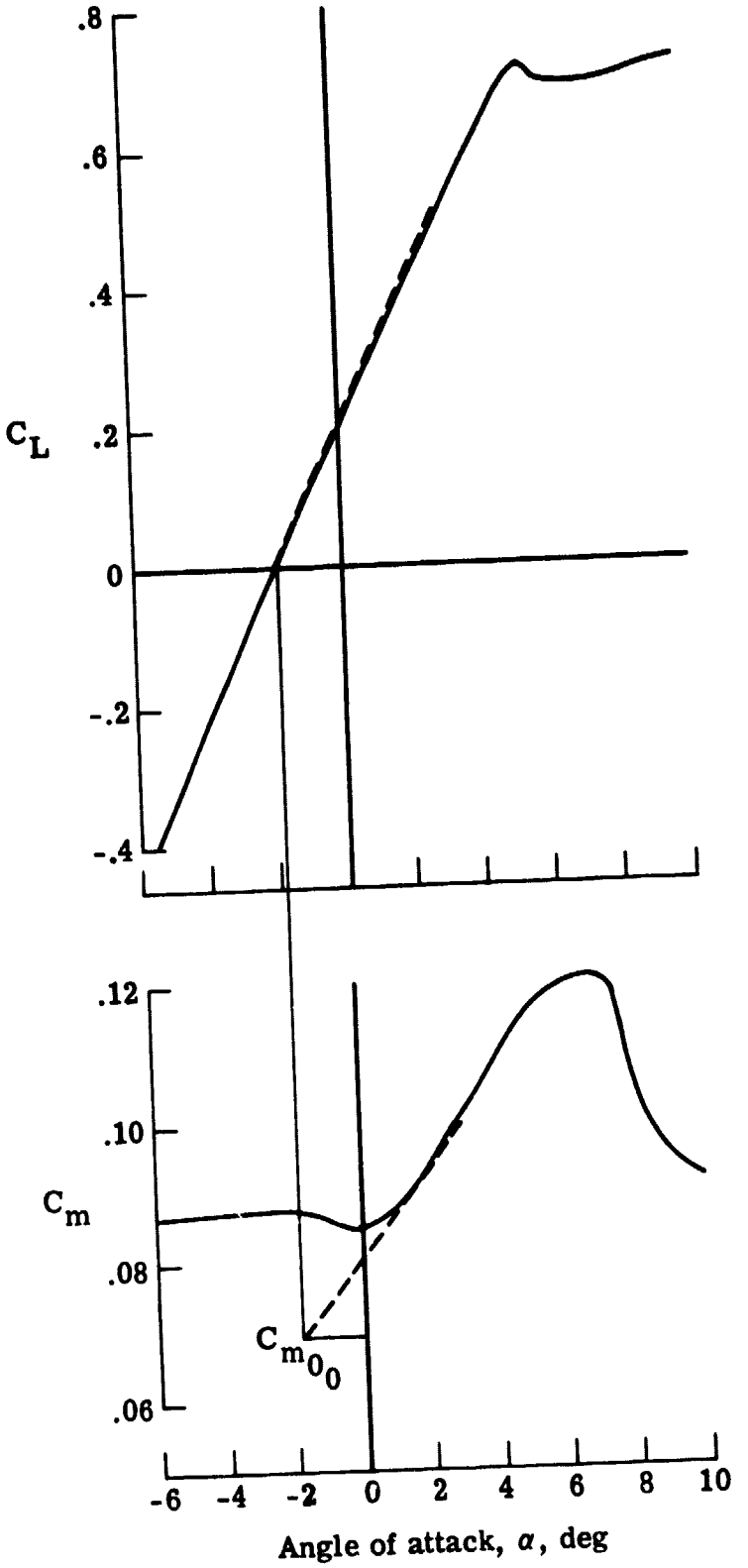

Figure 9.- ARW-2 Lift and moment coefficients as a function of angle of attack. Flight condition 6.

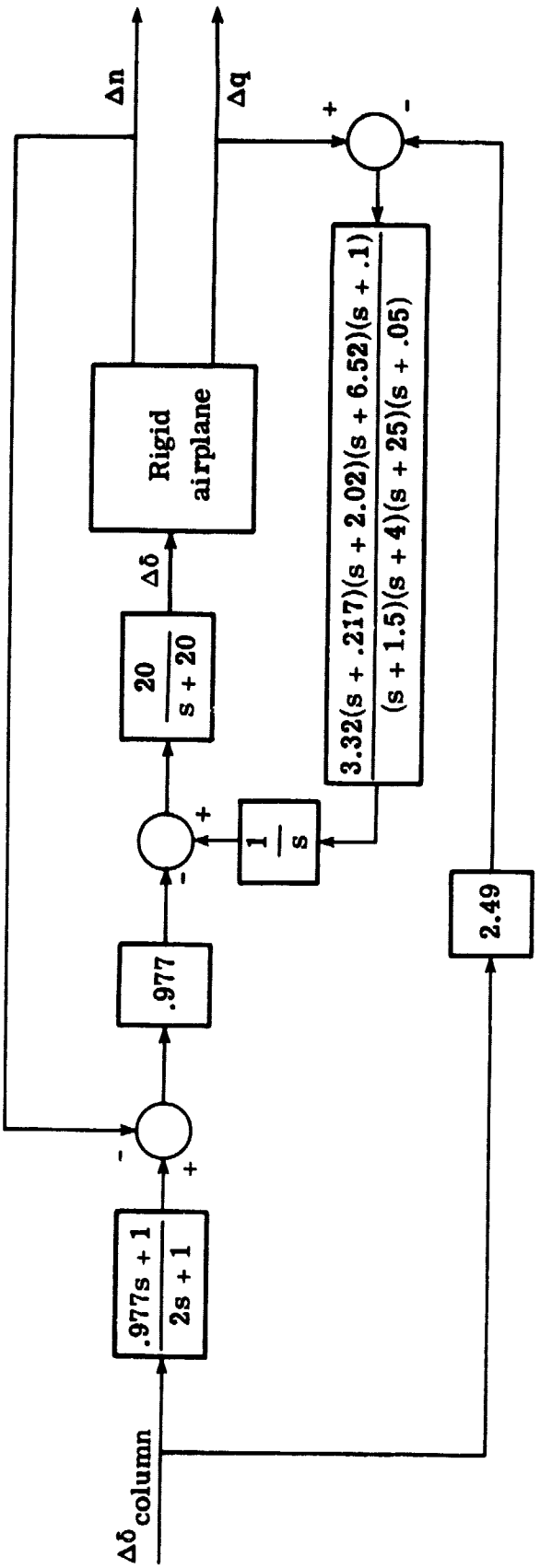

Figure 10.- Block diagram of AFCS and RSS system for ARW-2.
Gains correspond to Flight condition 6.

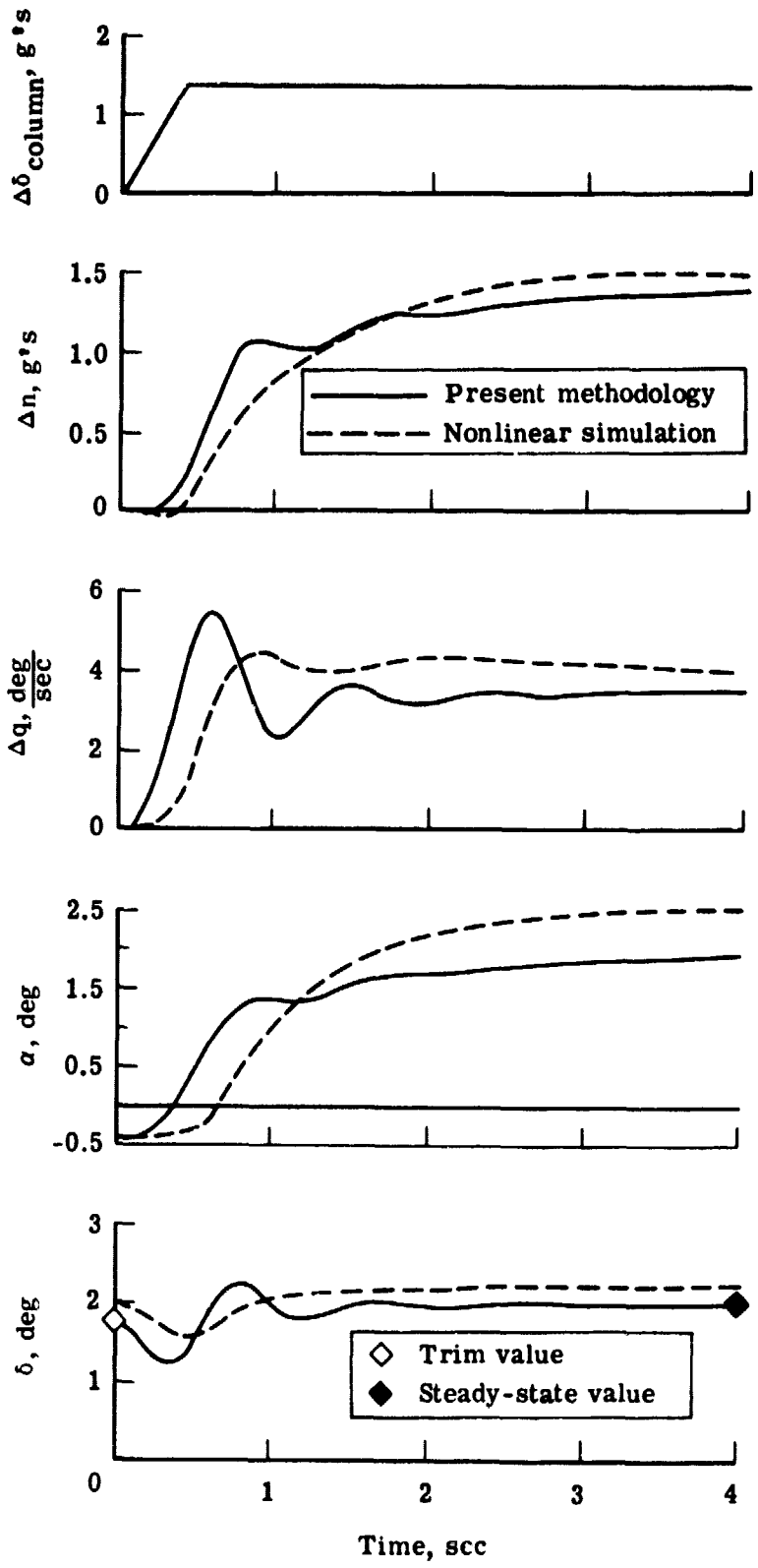

Figure 11.- Time histories for pull-up manuver.
Flight condition 6.